MCB Accepted Manuscript Posted Online 6 December 2021
Mol Cell Biol doi:10.1128/MCB.00363-21

Structure-guided approach to relieving transcriptional repression in Resistance to Thyroid Hormone α

Beatriz Romartinez-Alonso[1]*, Maura Agostini[2]*, Heulyn Jones[3], Jayde McLellan[3], Deepali Sood[3], Nicholas Tomkinson[3] , Federica Marelli[4], Ilaria Gentile[5], W. Edward Visser[2,6], Erik Schoenmakers[2], Louise Fairall[1], Martin Privalsky[2], Carla Moran[2], Luca Persani[4,5], Krishna Chatterjee[2]+, John Schwabe[1]+

[1]Leicester Institute of Structural and Chemical Biology, Department of Molecular and Cell Biology, University of Leicester, Leicester, UK.

[2]Wellcome Trust-MRC Institute of Metabolic Science, University of Cambridge, Cambridge, UK

[3]Department of Pure and Applied Chemistry, University of Strathclyde, Glasgow, UK

[4]Laboratory of Endocrine and Metabolic Research, IRCCS Istituto Auxologico Italiano, 20100 Milan, Italy

[5]Department of Medical Biotechnology and Translational Medicine, University of Milan, 20100 Milan, Italy

[6]Erasmus Medical Center, Department of Internal Medicine, Academic Center for Thyroid Diseases, Rotterdam, The Netherlands

*These authors contributed equally to this work

+ Coequal corresponding authors

Running title: Relieving mutant TRα-mediated repression in RTHα

Key words: Resistance to thyroid hormone; thyroid hormone receptor alpha; transcriptional repression

ABSTRACT

Mutations in thyroid hormone receptor α (TRα), a ligand-inducible transcription factor, cause Resistance to Thyroid Hormone α (RTHα). This disorder is characterised by tissue-specific hormone refractoriness and hypothyroidism, due to inhibition of target gene expression by mutant TRα-corepressor complexes. Using biophysical approaches, we show that RTHα-associated TRα mutants devoid of ligand-dependent transcription activation function, unexpectedly retain the ability to bind thyroid hormone. Visualisation of ligand (T3) within the crystal structure of a prototypic TRα mutant, validates this notion. This finding prompted synthesis of different thyroid hormone analogues, identifying a lead compound (ES08) which dissociates corepressor from mutant human TRα more efficaciously than T3. ES08 rescues developmental anomalies in a zebrafish model of RTHα and induces target gene expression in TRα mutation-containing cells from an RTHα patient, more effectively than T3. Our observations provide proof-of-principle for developing synthetic ligands that can relieve transcriptional repression by the mutant TRα-corepressor complex, for treatment of RTHα.

INTRODUCTION

The physiological effects of thyroid hormones (TH: thyroxine, T4; triiodothyronine T3), are mediated by its canonical action via nuclear thyroid hormone receptors (TRα, TRβ), with differing tissue distribution, which regulate transcription of target genes in a ligand-dependent manner[1]. Unliganded TRs recruit a multiprotein complex, containing corepressor (CoR, e.g. nuclear receptor corepressor, NCoR; silencing mediator of retinoic acid and thyroid hormone receptor, SMRT) and histone deacetylase (HDAC), to inhibit target gene transcription. Receptor occupancy by ligand (T3) promotes dissociation of this corepressor complex with relief of transcriptional repression, and mediates recruitment of a protein complex containing coactivators (e.g. NCoA-1/SRC-1; NCoA-2/GRIP-1; NCoA-3/ACTR) with chromatin remodelling activity, inducing transcription of target genes[2]. Short peptide sequences within these coregulators mediate interaction with receptor: both NCoR and SMRT contain multiple receptor interaction domains (RIDs) encompassing isoleucine-rich amphipathic motifs[3, 4, 5]; a leucine-rich (LXXLL) motif in coactivators mediates their binding to liganded receptor, with conserved hydrophobic residues in the carboxyterminal alpha helix (Helix 12; Fig 1b) of TR being critical for this interaction[6].

Heterozygous, loss-of-function mutations in human TRβ inhibit the function of their wild-type counterparts in a dominant negative manner, via a mechanism involving constitutive repression of target genes, to cause Resistance to Thyroid Hormone beta (RTHβ), a disorder characterised by elevated circulating thyroid hormones (TH) and non-suppressed pituitary TSH levels, consistent with hormone resistance and the predominant role of TRβ within the pituitary-thyroid feedback axis[7]. Conversely, RTHα due to heterozygous TRα mutations, manifests with features of hypothyroidism (skeletal dysplasia and growth retardation, neurocognitive impairment, low metabolic rate, reduced intestinal transit) reflecting hormone resistance in TRα-expressing tissues, but associated paradoxically with near-normal circulating TH levels. 19 different *THRA* defects have been recorded in 30 different families worldwide, with a significant subset (8/19) being frameshift or premature stop

mutations which disrupt the receptor carboxyterminus and are associated with a severe phenotype[8]. These TRα mutants are transcriptionally inactive, and fail to dissociate from corepressor or recruit coactivator, mediating potent dominant negative inhibition of wild-type receptor function[9,10,11].

CRISPR/Cas9 editing of *Thra* has generated several mouse lines, harbouring different frameshift/premature stop mutations disrupting the TRα carboxyterminus, which exhibit a hypothyroid phenotype homologous to RTHα; significantly, the phenotype is less severe in animals harbouring TRα mutants whose interaction with corepressor is reduced[12]. Crossing TRα-PV mice, another murine model of RTHα with mutant TRα carboxyterminus[13], with animals expressing defective *Ncor1* which cannot be recruited to TRα[14] or treating TRα-PV mice with suberoylanilide hydroxyamic acid (SAHA), a HDAC inhibitor[15] ameliorates phenotypes. Overall, these observations suggest that genetic or pharmacological disruption of the mutant TRα-CoR repression complex in RTHα might be beneficial.

Here, we have used biophysical (fluorescence anisotropy, circular dichroism) approaches to investigate molecular properties of TRα mutants. Unexpectedly we find that RTHα-associated TRα mutants can still bind T3. Validating this notion, we have visualised T3 within the crystal structure of a prototypic TRα mutant, homologous to RTHα-associated mutant receptors. This finding prompted us to design, synthesise and test TH analogues, identifying a lead compound which dissociated CoR from mutant human TRα more efficaciously than T3. This compound was more potent in preventing mutant human TRα-mediated developmental anomalies in a zebrafish model and induced greater TH target gene expression in patient-derived, TRα mutation-containing, primary cells studied *ex vivo*.

RESULTS

Biophysical analyses of TRα mutant-coregulator interactions

We studied three human TRα mutants (A382fs388X, F397fs406X, E403X) with disruption or truncation of the receptor carboxyterminus (Fig 1a, 1b), which constitutively repress TH target genes, fail to activate their transcription in response to T3 and inhibit wild-type receptor action in a dominant negative manner[9, 11], suggesting that their interaction with coregulator proteins is altered. To determine whether these mutations mediate failure of corepressor displacement or coactivator recruitment or a combination, we used a fluorescence anisotropy assay to investigate the ability of wild-type and mutant TRα ligand-binding domains (LBDs) to bind to peptide motifs derived from corepressor and coactivator receptor interaction domains, in the presence and absence of T3.

In the absence of T3, the interaction of both wild-type and mutant LBDs with the SMRT corepressor peptide is strong. Importantly, the mutant proteins (A382fs388X and F397fs406X) bind the corepressor with similar affinity to the unliganded wild-type receptor protein. In the absence of T3, neither wild-type nor mutant proteins exhibit detectable interaction with peptide from GRIP1 coactivator (Fig 2a).

As anticipated, the presence of saturating levels of T3 decreases the affinity of the wild-type TRα LBD for the SMRT corepressor peptide by almost 10-fold and also increases the affinity for coactivator peptide by several orders of magnitude (Fig 2a). These changes in coregulator affinity underlie the ligand-induced molecular switch (Fig 1b) which mediates the transition from repression to activation of target gene transcription by TR.

For TRα mutants, we have delineated two molecular defects: first, their affinity for corepressor in the presence of T3 is essentially unchanged; second, there is no T3 induced enhancement of coactivator interaction.

This behaviour of TRα mutants as if ligand were not present might suggest that the receptors are unable to bind to T3.

To test directly whether the mutant receptors are able to bind ligand we used a circular dichroism (CD) assay to monitor the thermal stability of the wild-type and TRα mutant LBDs in the presence and absence of saturating levels of T3 and coregulator peptides helix (Fig 2b). Interestingly, in the absence of ligand or coregulator peptides, A382fs388X and E403X TRα mutants exhibit slightly greater thermal stability compared to the wild-type receptor. This suggests that helix 12 in unliganded, wild-type TR may confer a destabilising effect which is not seen in TRα mutants lacking this carboxyterminal.

Strikingly, CD studies show that all three TRα mutants are able to bind to the ligand (T3) and show significant thermal stabilisation, similar to wild-type receptor. Similarly, in the absence of T3, both wild-type and mutant TRα proteins are significantly stabilised by corepressor binding. Significantly, for the three TRα mutants, the presence of both T3 and corepressor induced further stabilisation of proteins, strongly suggesting that both coregulator peptide and ligand can bind simultaneously to the receptor LBD (Fig 2b).

Given that all three TRα frameshift/truncation mutants lack helix 12 which caps the ligand binding pocket, with A382fs388X mutant TRα also lacking a significant portion of helix 11 which forms one side of the ligand binding pocket, the finding that all mutant LBDs are able to bind T3 was unexpected.

Since the CD experiments were performed with saturating T3 concentrations we determined the T3 binding affinity of the wild-type and mutant receptors in a competition assay using radiolabelled ligand (Fig 2c). This confirmed that all three mutants bind T3 with sub-micromolar affinity,

approximately 100-fold weaker than wild-type receptor. Together, these studies suggest that the mutations in these patient-derived receptors exert their effects through an impairment in ligand- and coregulator-binding equilibria (Fig 2d).

To assess the relative contribution of defective corepressor release versus coactivator recruitment to inhibition of TH action by mutant TRα, we analysed patient-derived primary cells containing E403X TRα, a mutant which exhibits both defective corepressor dissociation and coactivator recruitment, versus patient-derived cells containing E403K TRα, a mutant with predominantly defective coactivator interaction (Fig 3a). We observed that T3-dependent induction of KLF9, a TH target gene, was significantly more attenuated in E403X than E403K mutant TRα-containing cells (Fig 3b), supporting the concept that a receptor which cannot displace corepressor is more deleterious than one which simply cannot recruit coactivator. Importantly, electrophoretic mobility shift assays, using either canonical (DR + 4) or natural (human KLF9 promoter) thyroid response elements, showed that these differences in transcriptional activity were not due to differential DNA binding properties of E403X or E403K TRα mutants in the presence of natural (T3) or synthetic ligands (ES08, see below) (Fig 3c).

Structure of a ligand-bound mutant TRα.

To understand how the TRα mutants might bind ligand, we sought to crystallise the human mutant TRα LBDs in the presence of T3 and complexed with corepressor peptides, likely reflecting the dominant negative mutant receptor species *in vivo*. Unfortunately, we failed to obtain diffraction quality crystals, likely due to the presence of additional amino acids following frameshift mutations, which would be expected to be disordered. Accordingly, to model the human TRα mutants, we crystallised an artificial mutant receptor (P393GX), which is truncated at the carboxy terminus of helix 11 (Fig 4a, 4c).

Importantly, the P393GX TRα shows similar molecular behaviour to the human TRα mutants. In fluorescence anisotropy assays P393GX TRα interacts with corepressor peptides with comparable affinity to the human TRα mutant LBDs, with this interaction becoming stronger in the presence of T3 (Fig 5a). Similar to natural human TRα mutants, both ligand and corepressor peptide increase the thermal stability of P393GX TRα, with greatest stabilisation occurring in the presence of both T3 and SMRT-derived peptide, suggesting that P393GX LBD is able to bind T3 and SMRT corepressor simultaneously (Fig 5b). Radiolabelled ligand binding studies confirmed T3 binding to P393GX mutant TRα with micromolar affinity (Fig 2c), which was expected since the artificial mutant is more truncated than the natural, human TRα mutants.

Small crystals of P393GX in complex with T3 were obtained that diffracted to 3.0 Å. The structure contains one P393GX molecule (amino acids 156-393) and one molecule of T3 in the asymmetric unit (Fig 5c, Table 1). Much of the overall organization of the LBD is essentially the same as wild-type receptor protein. However, despite having the potential to form a complete helix 11 (αα 363-393), in P393GX mutant TRα this helix terminates at Ala 379 with the peptide backbone turning at this point to form an extended coil which runs antiparallel to the adjacent Helix 5 towards the corepressor-binding site.

The T3 ligand could be placed unambiguously in the hydrophobic cavity of P393GX TRα LBD (Fig 5d) and binds very similarly to its occupancy of wild-type receptor LBD (Fig 4d, 4e). However, T3 interactions with Met 388 and Phe 401 are lost and the orientation of His 381 is altered. Arg 384 makes a new interaction with the ligand in the P393GX LBD, donating a hydrogen bond to the 4' hydroxyl of the outer ring of T3. Interestingly, the lack of the carboxy terminal end of helix 11 and the loop joining to helix 12, creates space for residues amino terminal to helix 3 to form a short anti-parallel β-sheet that is not present in the wild-type receptor.

Remarkably, given that so much of the receptor carboxy-terminus is missing, the ligand binding cavity in P393GX mutant TRα is almost completely enclosed as a result of the rearrangement of the carboxy terminal portion of helix 11. Indeed, the volume of the ligand-binding cavity in P393GX is only slightly larger than that of the wild-type receptor (≈200 $Å^3$ *vs* is ≈160 $Å^3$ – as calculated using POCASA[16]). There is a small opening to the surface of the receptor around the 4' hydroxyl and iodine of the outer ring of T3, suggesting that the mutant receptor could likely accommodate a larger ligand in these positions. With P393GX mutant TRα being capable of binding T3 and corepressor (Fig 5b), we surmise that if the corepressor peptide binds receptor where expected, then part of the rearranged helix 11 would likely be displaced to accommodate this interaction.

Novel thyroid hormone analogues displace corepressor from human TRα mutants

The finding that both natural and artificial TRα mutant LBDs retain the ability to bind T3, raised the possibility that it might be possible to design novel ligands that are better able to displace corepressor, thereby alleviating transcriptional repression by mutant human TRα. We synthesised a series of ligands in which the hydroxyl group of T3 was modified with either ether, ester or sulfonate ester linkages of varying size, hydrophobicity and flexibility (Fig 6a).

Novel ligands were tested at saturating concentrations in fluorescence anisotropy and thermal stability assays with wild-type and human TRα mutant LBDs. In comparison to unliganded proteins, all compounds increased the thermal stability of wild-type and mutant LBDs, indicating their ability to bind these proteins. Strikingly, whereas T3 stabilized the wild-type TRα LBD better than synthetic analogues, several of the novel ligands (including ES08), stabilized mutant TRα proteins more effectively than T3, suggesting that the additional groups in these modified ligands enabled them to better occupy the aberrant ligand binding pockets of the mutant proteins (Fig 6b, lower panels). Fluorescence anisotropy assays measured the ability of ligands to perturb binding of wild-type and human TRα mutant LBDs to corepressor peptide (Fig 6b, upper panels). Many synthetic ligands

promoted dissociation of corepressor from wild-type TRα, but less effectively than T3, presumably due to their inability to rearrange helix 12 into its active, corepressor-displacing, conformation[17]. However, two compounds (ES08, ES09) mediated dissociation of corepressor from human TRα mutants more effectively than T3, particularly in the case of the mutant receptor E403X (6b, upper panels). Competition assays with radiolabelled T3, confirmed that both wild-type and E403X TRα were able to bind ES08 with sub-micromolar affinity. For wild-type TRα, ES08 binding is much weaker than T3. However, importantly, the E403X mutant TRα binds T3 and ES08 with similar affinity (Fig 7a).

Efficacy of TH analogues in mediating TRα-corepressor dissociation in cells

To compare the efficacy of T3 and synthetic ligands in promoting corepressor dissociation from TRα in cells, they were tested in cellular two-hybrid protein-protein interaction assays with coexpressed VP16-full length TRα and Gal4-corepressor fusions.

Both unliganded wild-type and mutant VP16-TRα fusion proteins exhibited strong interaction with Gal4-CoR fusions containing different isoforms of human NCoR (NCoR-ω, NCoR-δ) or SMRT (SMRT-α, SMRT-γ)[18]. T3 exposure readily dissociated all CoR isoform fusions from wild-type receptor but not human TRα mutants. SMRT-ε, a corepressor isoform lacking two receptor interaction motifs (S1, S3) did not interact with wild-type or mutant TRs (Fig 8a).

Next, we compared the relative efficacy of T3 versus different TH analogues (each at 100nM) in promoting corepressor dissociation from wild-type or mutant TRα, in the two-hybrid assays. In comparison to complete or partial dissociation of corepressor from wild-type receptor or TRα mutants with T3 exposure, most TH analogues exhibited comparable or inferior efficacy (Fig 8b). Notably, when tested with a particular human mutant receptor (E403X TRα), a single compound (ES08) promoted greater dissociation of corepressor from mutant TRα than T3 (Fig 8b, highlighted).

We confirmed that ES08 promotes greater corepressor dissociation from E403X mutant TRα than T3 when tested over a range of ligand concentrations (Fig 9a). Furthermore, in comparison to T3, ES08 also promotes greater dissociation of other corepressor isoforms (NCoR-ω, SMRT-α, SMRT-γ) from E403X mutant TRα (Fig 9b). However, neither ES08 or T3 were able to overcome the inability of E403X mutant TRα to recruit coactivator (Fig 9c).

Efficacy of TH analogue in E403X mutant TRα-expressing zebrafish and patient-derived primary cells

We evaluated the efficacy of ES08 versus T3 in a zebrafish model of RTHα, described previously[19]. Following microinjection of zygotes with either wild-type receptor or E403X mutant TRα mRNAs, embryos derived from E403X TRα mutant-injected zygotes exhibited multiple developmental anomalies, consisting of abnormal indices of morphology (AMI) vascular malformation (VMI) or skeletal malformation (SMI), whereas embryos from wild-type TRα-injected zygotes were unaffected (Fig 10).

Despite exposure to T3 at high concentrations (2-20μM), these developmental anomalies persisted in embryos derived from E403X TRα-injected zygotes, whereas their exposure to ESO8 (2μM) prevented morphological, vascular and skeletal malformations (Fig 10C, 10F, and 10K). Furthermore, in E403X mutant TRα-expressing embryos, lower concentrations of ES08 (2μM) induce greater expression of known thyroid hormone responsive target genes than high concentrations (2-20μM) of T3 (KLF9, Fig 11a; Dio3b, Fig 11b).

Finally, we compared the properties of ES08 versus T3 when incubated with primary, patient-derived, E403X mutant TRα-containing, inducible pluripotent stem cells. In comparison to T3, ES08 at higher concentration (2.5μM) induced greater expression of KLF9, a known thyroid hormone responsive target gene (Fig 11c).

DISCUSSION

Severe RTHα is caused by a molecular mechanism involving constitutive interaction of mutant TRα with corepressor, with failure of corepressor release and recruitment of coactivator in a ligand-dependent manner, silencing gene transcription. Unexpectedly, given unmeasurable radiolabelled T3 binding to mutant TRα in previous assays[9], our biophysical studies together with radiolabelled T3 binding assays showed that these human TRα mutants retain hormone binding. This notion was confirmed by visualising T3 within the crystal structure of an artificial TRα mutant, prototypic of receptor mutants that commonly cause RTHα. This finding prompted synthesis and evaluation of TH analogues, successfully identifying a single compound which dissociates corepressor from human mutant TRα more effectively than T3. This synthetic ligand prevents phenotypic abnormalities in a zebrafish model of RTHα and induces target gene expression in TRα mutation-containing cells from an RTHα patient, more efficaciously than T3.

The crystal structure of the P393GX TRα LBD reveals that the majority of the protein-ligand interactions are preserved in the mutant receptor despite the loss of much of H11 and H12. This accounts for why the mutant receptors retain ability to bind thyroid hormone – albeit with substantially reduced affinity. The position of the carboxy-terminal portion of H11 in the structure appears to occlude the CoR binding region. This would appear to be an artefact of crystallisation since we have shown experimentally that, like the natural TRα mutants, the P393GX receptor binds CoR both in the presence and absence of T3. We would predict that this region would not adopt a single conformation in solution.

Almost half (8/19) of the mutations causing RTHα which have been described hitherto are associated with a severe, hypothyroid phenotype and disrupt the receptor carboxy-terminus analogous to the TRα mutants we have studied here[9, 11, 20, 21, 22, 23]. To date, thyroxine treatment of such patients has been associated with a poor[10] or partial[11] clinical response. This may be due to the

fact that thyroxine therapy in conventional dosage does not lead to corepressor dissociation. New ligands that maximise the likelihood of corepressor dissociation from mutant TRα may be a more successful treatment.

Incomplete ligand-dependent release of corepressor from mutant TRα despite its ability to bind T3 therefore provided the rationale for synthesising TH analogues, identifying a compound (ES08) mediating greater corepressor displacement from the E403X mutant. ES08 and ES09 are sulfonate ester T3 analogues bearing a biaryl or 9*H*-fluorene substituent respectively. In the structure of ES08, it is possible that the change in geometry induced by the sulfonate ester link together with the relative rigidity of the extension sterically disrupts corepressor binding to the cleft on the TR LBD surface, thereby lowering its affinity for corepressor binding (Fig 7b, 7c). We speculate that the combination of a compound (ES08) which is most effective in changing conformation of the TRα LBD, together with preservation of part of helix 12 in E403X mutant TRα, accounts this analogue being able to displace corepressor most effectively from this particular TRα mutant.

One limitation of replacing the phenol group of T3 with a sulfonate ester in ES08, disrupting known interaction of its hydroxyl group with Histidine 381 in TR, may have been to compromise its receptor binding affinity. Accordingly, in the future, we will synthesise and test different ligands, restoring this phenol moiety and modifying T3 in the 5' position instead, with structural modelling suggesting that such analogues would be better orientated to displace corepressor. Furthermore, although the synthetic analogue we have identified (ES08) was only effective with a specific TRα mutant, our studies suggest that it may be possible to generate ligands that can better displace corepressor from this general subclass of mutant receptor. As the comparison of the E403X and E403K mutants suggests, corepressor displacement is beneficial even in the absence of coactivator recruitment. It is striking that corepressor-displacement, at high ES08 concentrations, has a significant beneficial effect in the Zebrafish model. Recent recognition that a thyroid hormone analogue

(triiodothyroacetic acid) which is used to treat Resistance to Thyroid Hormone β acts via this mechanism[24], provides added justification for this approach.

Other approaches to relieving transcriptional repression by the mutant TRα-corepressor complex in RTHα have limitations. In a recent study, abrogating NCoR-TR interaction in TRα-PV transgenic mice did not reverse skeletal abnormalities, supporting the notion that transcriptional repression by mutant TRα complexed with other corepressors (e.g. SMRT), may mediate this phenotype[25]. Similarly, targeting the TRα-corepressor repression complex pharmacologically with an HDAC inhibitor may not be effective if transcriptional repression operates via diverse complexes containing different HDACs that are not all sensitive to such inhibition[15]. Histone deacetylases are also components of complexes with other nuclear receptors and transcription factors[26, 27] and nonspecific inhibition of histone deacetylase enzyme activity may derepress these pathways, causing off target effects.

Overall, our observations provide a proof-of-concept for the synthesis of designer ligands, targeting aberrant mutant TRα-corepressor interaction, to alleviate receptor dysfunction in Resistance to Thyroid Hormone α.

MATERIALS AND METHODS

Expression and purification of TRα LBDs

The human WT, A382fs388X, F397fs406X, E403X and P393GX LBDs (residues 148-410, 148-387, 148-402 and 151-393) were cloned into a pGEX2T (GE Healthcare) vector containing an amino terminal GST purification tag followed by a TEV protease cleavage site. TRα LBDs were expressed in *E. coli* Rosetta (DE3) (Novagen) by growing the transformed Rosetta (DE3) at 37 °C in 2xTY until A_{595} = 0.1, then inducing with 40µM isopropyl-D-1-thiogalactopyranoside (IPTG) and grow overnight at 20°C. The bacterial cells were lysed by sonication in a buffer containing 1xPBS, 1 mM dithiothreitol (DTT) and complete EDTA-free protease inhibitor (Roche). The soluble protein was bound to glutathione sepharose (GE Healthcare), and washed with a buffer containing 1xPBS, 0.5% Triton X-100, 1mM DTT. Then the bound protein was washed with TEV cleavage buffer containing 20mM Tris-HCl pH 8, 100mM NaCl and 1mM DTT. GST tag was removed by incubation with TEV protease (100:1 molar ratio) overnight at 4°C.

Eluted proteins were loaded onto 5-ml HiTrap Q HP Ion Exchange column (HiTrap Q HP IEX), previously equilibrated in low salt buffer (20mM Tris-HCl pH 7.4, 50 mM NaCl, 1mM DTT). The protein was eluted with a 50-500nM NaCl gradient at a flow of 1.5ml/min. Partially purified samples were further purified on a Superdex 75 10/300 gel filtration column (GE Healthcare Bio-Science) in 30mM Tris-HCl pH 8.0, 50mM NaCl, 5% glycerol v/v, 1mM DTT, and 0.5mM EDTA. Pooled fractions were buffer exchanged and concentrated in 1xPBS, 1mM DTT buffer for fluorescence anisotropy and circular dichroism assays, and in 20mM Tris pH 8.0, 50 mM NaCl and 1mM of DTT for crystallisation studies.

Radiolabelled T3 binding assays

Homologous competitive binding assays were performed using Triiodothyronine (T3) labeled with ^{125}I (^{125}I-T3, PerkinElmer). Recombinant WT, mutant and artificial mutant TRα LBDs were incubated

with 0.02nM ^{125}I-T3 in binding buffer (20mM Tris pH 8, 50mM KCl, 1mM $MgCl_2$, 10% glycerol, 5mM DTT) in the presence of increasing amounts of unlabelled competing T3 (0-100µM). Appropriate protein concentration was determined experimentally to give 10% of the total radioactivity of the assay securing a good signal (total binding) to noise (non-specific binding) ratio, and preventing the ligand depletion effect. Following 1 hour of incubation at 37°C, bound T3 was separated from unbound T3 by passage through a filter membrane (Millipore HA filters, 0.45µ) under vacuum followed by three washes with 2ml of ice-cold binding buffer. Filters containing TR-bound ^{125}I-T3 was measured in a γ-counter.

Competitive binding assay was performed following the same procedure in the presence of increasing amounts of unlabelled competing ES08 (0-10µM) using recombinant WT and E403X TRα LBDs.

A half maximal inhibitory concentration (IC_{50}), which indicates amount of ligand that causes 50% inhibition of radioligand binding, is obtained by plotting the radioactivity values obtained at every cold competing T3 concentration using the GraphPad Prism and a nonlinear regression analysis. Since the dissociation constant, Kd, and the inhibitor constant, Ki, should be the same as the radioactive ligand and the competing ligand are the same, in this type of experiments the Kd of the binding is calculated by subtracting the concentration of radioligand from the IC_{50} value obtained from the curve as follows: $Kd = Ki = IC_{50} - [radioligand]$.

Fluorescence anisotropy and circular dichroism

Two peptides were designed for using in the fluorescence anisotropy assay. An N-terminal FITC labelled 14-aa length peptide with sequence based on the interaction domain 1 of the SMRT corepressor protein (RID1 residues 2346-2360: Ac-STNMG**L**EA**I**IRKA**L**MG-NH_2), containing the corepressor NR recognition motif LxxxIxxx[I/L]; and a C-terminal BODIPY-TMR labelled 16-aa length

peptide with sequence based on the second NR interaction box of GRIP1 coactivator protein (NID2 residues 686-700: Ac-KHKI**L**HR**LL**QDSSC-NH_2) containing the coactivator NR recognition motif LxxLL.

Fluorescence anisotropy (FA) experiments were performed in black 96-well assay plates (Corning Life Sciences). Multiple titrations were performed using fixed concentration of SMRT and GRIP1 peptides (5nM) with increasing concentrations of TRα LBDs (0-5μm) in a final volume of 50μl of assay buffer (1xPBS, 0.01% (v/v) Triton X-100, 0.1 mg/ml BSA). For the assays in the presence of T3 or T3 analogues, increasing concentrations of the mixture protein:T3 or protein:T3 analogues in a 1:2 molar ratio were used. After incubation at room temperature for 5 minutes with slow shaking and centrifugation of the plates, the FA value was measured at each receptor concentration in a Victor X5 multilabel plate reader (Perkin Elmer, Singapore) using a 480-nm excitation filter and 535-nm emission filters to measure FITC emission and 542-nm excitation filter and 572-nm emission filters to measure BODIPY fluorescence. Blank fluorescence values were subtracted in each polarization plane. FA values obtained at every protein concentration were used to generate saturation binding curves that subsequently were used to calculate the equilibrium dissociation constant of the interaction (Kd), using the Prism software (Graphpad) and the nonlinear regression analysis.

Thermal unfolding of proteins was monitored by CD spectroscopy, over a wavelength range of 200-250 nm, using a Chirascan Spectrometer (Applied Photophysics) equipped with a temperature controller (Quantum Northwest TC125). CD spectra were measured from samples in 1 mm path length quartz cuvettes, using a scanning speed of 100 nm/min, a spectral bandwidth of 1 nm, and a response time of 1 second. Secondary structure of the proteins was assessed by visual inspection of CD spectra from 200-250 nm. The thermal denaturation or unfolding profile of the proteins was characterized by measuring the ellipticity changes at 222 nm induced by a temperature increase from 20 to 90°C at steps of 1 degree.

Peptide synthesis

SMRT and GRIP1 peptides were synthesised using a CEM Liberty 1 automated microwave peptide synthesizer on a 0.05µmol scale, using solid phase peptide synthesis (SPPS). In this technique, an N-protected C-terminal amino acid residue is anchored to an amino resin, in this case H-Rink Amide Chem Matrix resin.

The amino acids were loaded onto this resin in a sequential manner from the C-terminus to the N-terminus by repetitive cycles. Amino acids were Fmoc-protected and solubilized in DMF to a concentration of 0.2M. After loading every amino acid, they were deprotected using 20% piperidine in DMF to remove the Fmoc group. 0.5M HCTU in DMF was used as the activator with 3M DIPEA in NMP (N-Methyl-2-pyrrolidone) as an activator base. The deprotection and amino acid coupling reactions were repeated in a linear manner for each amino acid to build the peptide sequence from C-terminus to N-terminus.

After synthesis of the full peptide sequences, the resin was removed and washed. For the SMRT peptide, it was incubated with Fluorescein Isothiocyanate (FITC) in 5-fold molar excess for 5 hours on a shaker at room temperature. FITC-SMRT peptide and GRIP1 peptide were cleaved from the resin by incubating the resin in 1mL of TFA:TES:H_2O at room temperature for 3 hours. The peptides were precipitated using cold diethyl ether and then centrifuged at 3500 x g for 5 minutes. Supernatants were discarded and the pellets were washed twice more with diethyl ether. After the 3rd ether wash the peptides were freeze-dried and left overnight before purification using semi-prep HPLC. The fractions containing peptide from HPLC were pooled and a sample was submitted for LC-MS to determine purity.

BODIPY-TMR C_5 malemide (Invitrogen) was coupled to GRIP1 peptide after the synthesis through and N-terminal cysteine. 90µM peptide was incubated with a 5-fold molar excess of BODIPY in a 1ml reaction with constant stirring for 2 hours in darkness at room temperature. The purification of the

labelled peptide from free dye was performed using a PD-10 column (GE Healthcare) pre-equilibrated with 1xPBS containing 0.5% TCEP. Eluted fractions were concentrated to 50µl using an Amicon centrifugal concentrator.

Crystallisation, structure determination and refinement

The P393GX LBD was mixed with a 5-fold molar excess of T3 (Sigma) and concentrated up to 9 mg/ml. Crystallisation trials were initially conducted using commercial screens (Molecular Dimensions) into MRC 96 well sitting drop crystallisation plates using 100nl of protein sample and precipitant. Hexagonal crystals up to 20-µm length were grown by sitting drop vapour diffusion at room temperature using 0.2M NaCl 0.1M Tris pH 8.5 and 1M Lithium Sulphate. Prior to analysis, cryoprotectant solution containing the crystallisation conditions with the addition of glycerol to 20% was added to the crystals which were then rapidly frozen at 100K using liquid nitrogen. Data was collected at the microfocus beamline I-24 at the Diamond Light Source (UK). The structure was solved by molecular replacement using wild-type TRα LBD (PDB code 2h79) as a search model in Phaser. The preliminary model was rebuilt iteratively by multiple rounds of refinement and building using Refmac5 and Coot to a R_{free} of 22% and a R_{work} of 18%. The final model contains one molecule of P393GX and one molecule of T3 in the asymmetric unit. The final model has 95.73% residues in the favoured region, 4.27% in the allowed regions and none in the outlier region of the Ramachandran plot (Suppl Table 1).

Synthesis of TH analogues

Protection of T3: *tert*-butyl (*S*)-2-((*tert*-butoxycarbonyl)amino)-3-(4-(4-hydroxy-3-iodophenoxy)-3,5-diiodophenyl)propanoate. To a solution of T3 (1.20 g, 1.84 mmol) in *tert*-butyl acetate (4.40 mL, 0.033 mol, 18 equiv) at 0 °C was added perchloric acid (0.67 mL, 11.06 mmol, 6 equiv) drop-wise.

Upon completion of addition, the cooling bath was removed, and the reaction mixture stirred for 1 h at room temperature. The reaction mixture was cooled to -10 °C and excess acid neutralised by the very slow drop-wise addition of a solution of potassium carbonate (3.06 g, 0.022 moles, 12 equiv) in water (5.0 mL), keeping the temperature below 0 °C. THF:water (1:1, 6.0 mL) and a solution of potassium carbonate (0.51 g, 3.69 mmol, 2 equiv) in water (1.0 mL) were added followed by the slow drop-wise addition of a solution of Boc anhydride (0.443 g, 2.03 mmol, 1.1 equiv) in THF (6.0 mL). The reaction mixture was warmed to room temperature and stirred for 2.5 h. The reaction mixture was extracted with EtOAc (3 × 30 mL), the combined organic extract dried over magnesium sulfate, filtered and concentrated under reduced pressure to afford the crude product, which was purified by flash chromatography on silica (petroleum ether (40 – 60 °C): ethyl acetate, 3:1) to give the protected T3, as a white solid (899 mg, 1.11 mmol, 60%). MP: 85-86 °C; FTIR (ATR/cm^{-1}) υ_{max}: 3355, 2968, 2932, 1703, 1688, 1577, 1508, 1441; ^{1}H NMR (400 Hz, $CDCl_3$): δ 7.66 (s, 2H), 7.08 (d, *J* = 3 Hz, 1H), 6.89 (d, *J* = 9 Hz, 1H), 6.66 (dd, *J* = 3, 9 Hz, 1H), 5.15 (d, *J* = 6 Hz, 1H), 4.42–4.40 (m, 1H), 3.06–2.94 (m, 2H), 1.46 (s, 9H), 1.45 (s, 9H); ^{13}C NMR (100 Hz, $CDCl_3$): δ 170.4, 156.0, 153.0, 150.6, 150.3, 141.4, 138.0, 124.8, 117.4, 115.3, 90.8, 85.4, 83.1, 80.3, 54.8, 37.1, 28.2, 28.2. LRMS: (LC-MS) *m/z* calc. 806.91 $[M+H]^+$, *m/z* found 805.8 $[M-H]^+$.

Protected ES08: *tert*-butyl (*S*)-3-(4-(4-(([1,1'-biphenyl]-4-ylsulfonyl)oxy)-3-iodophenoxy)-3,5-diiodophenyl)-2-((*tert*-butoxycarbonyl)amino)propanoate. To a stirred solution of protected T3 (75 mg, 0.09 mmol) in anhydrous dichloromethane (4.0 mL) were added (75 mg, 0.09 mmol)at room temperature under a nitrogen atmosphere. The resulting solution was stirred at room temperature for 16 h. The reaction mixture was quenched with water (15 mL) and the aqueous phase extracted with dichloromethane (3 × 30 mL). The organic layers were combined and washed with saturated sodium hydrogen carbonate solution (20 mL) and brine (20 mL). The organic layers were dried over magnesium sulphate, filtered and concentrated under reduced pressure. Purification by flash column chromatography on silica (petroleum ether (40–60 °C):ethyl acetate, 5:1) afforded the *title*

compound as a white solid (67 mg, 0.065 mmol, 71%). ^{1}H NMR (400 Hz, $CDCl_3$): δ 7.92 (d, *J* = 8 Hz, 2H), 7.69 (d, *J* = 8 Hz, 2H), 7.63 (s, 2H), 7.58 (d, *J* = 7 Hz, 2H), 7.47–7.40 (m, 3H), 7.23 (d, *J* = 4 Hz, 1H), 7.12 (d, *J* = 3 Hz, 1H), 6.69 (dd, *J* = 3, 9 Hz, 1H), 5.10 (d, *J* = 6 Hz, 1H), 4.37 (app d, *J* = 5 Hz, 1H), 3.03–2.90 (m, 2H), 1.41 (s, 9H), 1.41 (s, 9H); ^{13}C NMR (100 Hz, $CDCl_3$): δ 170.3, 167.5, 154.7, 152.4, 147.6, 145.2, 141.5, 139.0, 138.5, 134.2, 129.6, 129.3, 129.0, 127.8, 127.6, 126.8, 123.7, 116.5, 90.4, 90.9, 83.1, 80.3, 54.8, 37.1, 28.2, 28.5.

ES08: (*S*)-3-(4-(4-(([1,1'-biphenyl]-4-ylsulfonyl)oxy)-3-iodophenoxy)-3,5-diiodophenyl)-2-aminopropanoic acid. Protected **ES08** (53 mg, 0.052 mmol) was introduced to a microwave vial and water:acetic acid (1:1, 0.52 mL) was added. The microwave vial was heated at 160 °C for 20 min in a BIOTAGE microwave and then cooled to room temperature. The deprotection was monitored by LCMS analysis. The resultant mixture was transferred into a round bottom flask using a minimal volume of water. The mixture was concentrated under reduced pressure using a freeze dryer in order to remove residual water and acetic acid to give **ES08**, as an off-white solid (18 mg, 0.021 mmol, 40%). MP: 209-212 °C; FTIR (ATR/cm^{-1}) υ_{max}: 3062, 2960, 2922, 1701, 1593, 1541, 1472; ^{1}H NMR (400 Hz, DMSO): 8.01 (d, *J* = 8 Hz, 2H), 7.90 (d, *J* = 8 Hz, 2H), 7.83 (s, 2H, 2), 7.80 (d, *J* = 7 Hz, 2H), 7.57–7.47 (m, 3H), 7.21 (d, *J* = 9 Hz, 2H), 6.87 (dd, *J* = 2, 9 Hz, 1H), 3.12 (dd, *J* = 3, 14 Hz, 1H), 2.84–2.97 (m, 2H); LRMS**:** (LC-MS) *m/z* calc. 886.81 $[M+H]^+$, *m/z* found 865.7 $[M-H]^+$.

Electrophoretic mobility shift and two-hybrid protein-protein interaction assays

Electrophoretic mobility shift assays, using WT, E403X and E403K mutant TRα proteins and RXRα and either canonical or human KLF9 promoter TREs[28], were undertaken as described previously[9].

For expression in transiently transfected mammalian cells, full length WT and mutant TRα cDNAs were cloned in pCMX-VP16 (kind gift from R. Evans) to yield VP16-TRα fusions. Constructs expressing the GAL4 DNA-binding domain (GAL4DBD) alone, or fused to receptor-interacting domains of SMRT or NCoR corepressor isoforms and TRAP220 coactivator have been previously described[29, 30, 31]. The

523 reporter gene (UASTKLUC) containing GAL4 binding sites and vector (Bosβ-gal) used to correct for
524 transfection efficiency, have also been previously described[32].
525
526 Human embryonic kidney cells (HEK293), seeded in medium (DMEM supplemented with 10%
527 charcoal-stripped FBS and 1% PSF (GIBCO-Invitrogen), were transfected using Lipofectamine 2000
528 (Invitrogen) with 16ng of Gal4DBD-cofactor, 8ng of VP16-TRα1, 80ng UASTKLUC and 8ng Bosβgal
529 expression vectors. Following exposure to fresh medium supplemented with either vehicle (DMSO),
530 T3 or different thyroid hormone analogues, cells were harvested 36hrs later and luciferase activity
531 normalised to Bosβgal activity. Results shown are the mean +/- SEM of at least 5 independent
532 experiments each performed in triplicate.
533
534 **Zebrafish studies**
535 Zebrafish (*Danio rerio*) from wild-type (AB) and *tg*(*kdrl*:EGFP) adults were maintained in controlled
536 conditions and all procedures conformed to Italian law (D. Lgs n° 2014/26, implementation of the
537 2010/63/UE). WT and E303X mutant human *THRA* (ENST00000450525) vectors were linearized and
538 transcribed *in vitro* using the mMESSAGE mMACHINET7 kit (Ambion) and RNA purified using the
539 Megaclear kit (Ambion). Zebrafish eggs (1-2 cell stage), were injected with hTRα1 transcripts (WT or
540 E403X mutant) at a dose of 80 pg/embryo. 6 hours-post fertilization, the injected embryos were
541 treated with 20µM DMSO (Sigma), 2-20µM triiodothyronine (IBSA-Farmaceutici) or 0.5-2µM ES08,
542 added to the harvesting water. Morphological (cerebral oedema, cardiac oedema, altered body
543 curvature, thinning of caudal vein plexus), vascular (incomplete formation, misplaced, or aberrant
544 branching of intersomitic vessels, and reduced area of caudal vein plexus) and skeletal (reduced or
545 loss of mineralization of cleitrum and operculum, defective ceratohyal arch and ceratobranchial
546 cartilages) anomalies were graded (0=normal, or 1 to 4= increasingly abnormal) and used to
547 compute an abnormal morphological index (AMI), vascular malformation index (VMI) or skeletal

malformation index (SMI). Expression of known thyroid hormone responsive target genes in zebrafish[33, 34]was measured by quantitative real-time PCR as described previously[19].

***Ex vivo* studies of patient-derived peripheral blood mononuclear cells and inducible pluripotent stem cells**

Human inducible pluripotent stem cells (hIPSCs) were derived from primary, peripheral blood mononuclear cells of the RTHα patient with the E403X TRα mutation[9] by our NIHR BRC hIPSC core facility as described previously[35]. Following exposure of cultured peripheral blood mononuclear cells or hiPSCs to T3 or analogue, expression of KLF9, a thyroid hormone receptor target gene, was quantified as described previously[9].

Statistical analysis

Comparisons of data were undertaken using unpaired, 2-tailed t tests throughout. P values of less than 0.05 were considered significant.

564 **REFERENCES**

565 1. Lazar, M.A. Thyroid Hormone Receptors: Multiple forms, multiple possibilities. *Endocr. Rev.* **14**,
566 184–193 (1993).

567 2. Horlein, A.J., Heinzel, T., Rosenfeld, M.G. Gene regulation by thyroid hormone receptors. *Curr.*
568 *Opin. Endocrinol. Diab.* **3**, 412–416 (1996).

569 3. Nagy, L., *et al*. Mechanism of corepressor binding and release from nuclear hormone receptors.
570 *Genes Dev.* **13**, 3209-3216 (1999).

571 4. Hu, X., & Lazar, M.A. The CoRNR motif controls the recruitment of corepressors by nuclear
572 hormone receptors. *Nature* **402**, 93-96 (1999).

573 5. Perissi, V., *et al*. Molecular determinants of nuclear receptor-corepressor interaction. *Genes Dev.*
574 **13**, 3198-3208 (1999).

575 6. Heery, D. M., Kalkhoven, E., Hoare S., & Parker, M. G. A signature motif in transcriptional co-
576 activators mediates binding to nuclear receptors. *Nature* **387**, 733-736 (1997).

577 7. Refetoff, S., & Dumitrescu, A.M. Syndromes of reduced sensitivity to thyroid hormone: genetic
578 defects in hormone receptors, cell transporters and deiodination. *Best Pract. Res. Clin. Endocrinol.*
579 *Metab.* **21**, 277-305 (2007).

580 8. Moran, C., & Chatterjee, K. Editorial: Resistance to Thyroid Hormone α- emerging definition of a
581 disorder of thyroid hormone action. *J. Clin. Endocrinol. Metab.* **101**, 2636-2639 (2016).

582 9. Bochukova, E., *et al*. A mutation in the thyroid hormone receptor alpha gene. *N. Engl. J. Med.* **366**,
583 243-249 (2012).

584 10. van Mullem, A. A., *et al*. Clinical phenotype of a new type of thyroid hormone resistance caused
585 by a mutation of the TRα1 receptor: consequences of LT4 treatment. *J. Clin. Endocrinol. Metab.* **98**,
586 3029-3038 (2013).

587 11. Moran, C., *et al*. An adult female with resistance to thyroid hormone mediated by defective
588 thyroid hormone receptor α. *J. Clin. Endocrinol. Metab.* **98**, 4254-4261 (2013).

12. Markossian, S., *et al*. CRISPR/Cas9 editing of the mouse *THRA* gene produces models with variable resistance to thyroid hormone. *Thyroid* **28**, 139-150 (2018).

13. Kaneshige, M., *et al*. A targeted dominant negative mutation of the thyroid hormone alpha 1 receptor causes increased mortality, infertility, and dwarfism in mice. *Proc. Natl. Acad. Sci. USA* **98**, 15095-15100 (2001).

14. Fozzatti, L., *et al*. Nuclear receptor corepressor (NCOR1) regulates in vivo actions of a mutated thyroid hormone receptor α. *Proc. Natl. Acad. Sci. USA* **110**, 7850-7855 (2013).

15. Kim, D. W., Park, J. W., Willingham, M. C., & Cheng, S-Y. A histone deacetylase inhibitor improves hypothyroidism caused by a TRα1 mutant. *Hum. Mol. Genet.* **23**, 2651-64 (2014).

16. Yu, J., Zhou, Y., Tanaka, I., & Yao, M. Roll: a new algorithm for the detection of protein pockets and cavities with a rolling probe sphere. *Bioinformatics*, **26,** 46-52 (2010).

17. Lin, B. C., Hong, S-H., Krig, S., Yoh, S. M., & Privalsky, M. L. A conformational switch in nuclear hormone receptors is involved in coupling hormone binding to corepressor release. *Mol. Cell. Biol.* **17**, 6131-6138 (1997).

18. Goodson, M. L., Mengeling, B. J., Jonas, B. A., & Privalsky, M. L. Alternative mRNA splicing of corepressors generates variants that play opposing roles in adipocyte differentiation. *J. Biol. Chem.* **286**, 44988-44999 (2011).

19. Marelli, F., Carra, S., Rurale, G., Cotelli, F., & Persani, L. *In vivo* functional consequences of human THRA variants expressed in the zebrafish. *Thyroid* **27**, 279-291 (2017).

20. van Mullem, A., *et al*. Clinical phenotype and mutant TRα1. *N. Engl. J. Med*. **366**, 1451-1453 (2012).

21. Tylki-Szymanska, A., *et al*. Thyroid hormone resistance syndrome due to mutations in the thyroid hormone receptor α gene (*THRA*). *J. Med. Genet.* **52**, 312-316 (2015).

22. Demir, K., *et al*. Diverse genotypes and phenotypes of three novel thyroid hormone receptor alpha mutations. *J. Clin. Endocrinol. Metab.* **101**, 2945-2954 (2016).

23. Sun, H., *et al*. New case of thyroid hormone resistance α caused by a mutation of THRA/TRα1. *J. Endocr. Soc.* **3**, 665-669 (2019).

24. Harrus, D., *et al*. Pathological interactions between mutant thyroid hormone receptors and corepressors and their modulation by a thyroid hormone analogue with therapeutic potential. Thyroid **28**, 1708-1722 (2018).

25. Freudenthal, B., *et al*. Genetic and pharmacological targeting of transcriptional repression in resistance to thyroid hormone alpha. *Thyroid* **29**, 726-734 (2019).

26. Nagy, L., & Schwabe, J.W. Mechanism of the nuclear receptor molecular switch. *Trends Biochem. Sci.* **29**, 317-324 (2004).

27. Emmett, M.J., & Lazar, M.A. Integrative regulation of physiology by histone deacetylase 3. *Nat. Rev. Mol. Cell. Biol.* **20**, 102-115 (2019).

28. Denver, R.J., Williamson, K.E. Identification of a thyroid hormone response element in the mouse kruppel-like factor 9 gene to explain its postnatal expression in the brain. Endocrinology. 150, 3935-3943 (2009).

29. Wong, C.W., & Privalsky, M.L. Transcriptional silencing is defined by isoform- and heterodimer-specific interactions between nuclear hormone receptors and corepressors. *Mol. Cell Biol.* **18**, 5724-5733 (1998).

30. Horlein, A.J., *et al*. Ligand-independent repression by the thyroid hormone receptor mediated by a nuclear receptor co-repressor *Nature* 377, 397-403 (1995).

31. Yuan, C.X., Ito, M., Fondell, J.D., Fu, Z.Y., Roeder, R.G. The TRAP220 component of a thyroid hormone receptor- associated protein (TRAP) coactivator complex interacts directly with nuclear receptors in a ligand-dependent fashion. *Proc. Natl. Acad. Sci. USA.* **95**, 7939-7944 (1998). Erratum in: Proc Natl Acad Sci USA 24, 14584 (1998).

32. Collingwood, T.N., *et al*. A role for helix 3 of the TRbeta ligand-binding domain in coactivator recruitment identified by characterization of a third cluster of mutations in resistance to thyroid hormone. *EMBO J.* **17**, 4760-4770 (1998).

640 33. Zhang, Y., *et al*. Thyroid hormone regulates hematopoiesis via the TR-KLF9 axis. Blood. 130, 2161-
641 2170 (2017).
642 34. Walter, K.M., *et al*. Effects of thyroid hormone disruption on the ontogenetic expression of
643 thyroid hormone signalling genes in developing zebrafish (Danio rerio). *Gen. Comp. Endocrinol*. 272,
644 20-32 (2019).
645 35. Agu, C.A., *et al*. Successful Generation of Human Induced Pluripotent Stem Cell Lines from Blood
646 Samples Held at Room Temperature for up to 48 hr. *Stem Cell Reports*. 2015 **5**, 660-71 (2015).
647

ACKNOWLEDGMENTS

Our research is supported by the Wellcome Trust (Investigator Award 210755/Z/18/Z to KC; Investigator Award 100237/Z/12/Z to JS) and NIHR Cambridge Biomedical Research Centre (CM, KC). JS is a Royal Society Wolfson Research Merit Award Holder. Zebrafish studies (FM, LP) were supported by Ricerca Corrente Funds (Transtir, 05C501_2015) of Istituto Auxologico Italiano and an unrestricted research grant from Sandoz, Italy. WEV was supported by a Marie Curie Intra-European Fellowship (330183) and a research grant from the Foundation for Development of Internal Medicine in Europe. We are particularly grateful to John Challiss for advice and assistance with the radioligand-binding assays.

AUTHOR CONTRIBUTIONS

JS, KC, NT, LP, BR-A, MA, FM conceived the project and designed experiments. BR-A performed fluorescence anisotropy, circular dichroism assays and radiolabelled ligand-binding assays, crystallised mutant thyroid receptor and solved the structure with assistance from LF. HJ, JM, DS and NT synthesised thyroid hormone analogues. MA and EV and ES undertook two-hybrid protein interaction assays and gene expression studies. FM, IG and MA performed zebrafish and pluripotent stem cell experiments. BR-A, MA, NT, MP, CM, LP, KC and JS wrote and edited the manuscript.

COMPETING INTERESTS

The authors declare no competing interests.

NAME AND ADDRESS OF CORRESPONDING AUTHORS:

Name: John Schwabe

Address: Leicester Institute of Structural and Molecular Biology, Department of Molecular and Cell Biology, University of Leicester, Leicester, UK.

Phone: (44)-116 – 229 7030

Email: js336@le.ac.uk

OR

Name: Krishna Chatterjee

Address: Metabolic Research Laboratories, Institute of Metabolic Science, Level 4, Box 289,

Addenbrooke's Hospital, Cambridge, CB2 0QQ

Phone: (44)-1223-336842

Email: kkc1@medschl.cam.ac.uk

FIGURE LEGENDS

Figure 1. Location of human TRα mutations and WT TRα molecular switch (a) Schematic representation of the full-length TRα, denoting the different functional domains of the receptor. Location of natural human mutations associated with RTHα (A382fs388X, F397fs406X and E403X) and artificial mutation (P393GX) made for crystallization studies is indicated. **(b)** Structural model of TRα hormone binding domain (PDB 2h79) in the unliganded state interacting with corepressor peptide (red) from the PPARα LBD:SMRT complex (PDB 1kkq) (left panel), and in the liganded state bound to coactivator peptide (blue) from the PPARα LBD:GRIP1 complex (pdb code: 1p54) (right panel). The position (A382, F397, E403) of natural human TRα mutations and hydrogen bond between E403 and coactivator peptide is also shown.

Figure 2. Interaction of human TRα mutants with corepressor and coactivator peptides (a) Binding affinities (dissociation constants) of wild-type and mutant TRα LBDs for corepressor in the absence (red square, white fill) and presence (red square, red fill) of T3 and for coactivator in the absence (blue square, white fill) and presence (blue square, blue fill) of T3 in fluorescence anisotropy assays. Error bars indicate mean ± s.e.m. (n=5); **p< 0.01. **(b)** Thermal stability (melting temperature) of wild-type and mutant TRα LBDs alone (black square, white fill) in the presence of T3 (black fill), with SMRT corepressor peptide (red square, white fill) or with both SMRT and T3 (red square, red fill). Error bars indicate ± s.e.m. (n=5); *p<0.05, **p< 0.01. **(c)** Radiolabelled T3 competitive binding assays of wild-type, mutant and artificial mutant TRα showing the dissociation curves in the presence of increasing concentration of unlabelled T3, and the dissociation constant (Kd) obtained. Data presented as mean ± s.e.m. from two independent experiments performed in triplicate. **(d)** Scheme summarising how the patient-derived mutations perturb the equilibria between ligand- and coregulator-bound species.

Figure 3. Comparison of the behaviour of E403X and E403K mutant TRα receptors. (a) Two-hybrid

assay to investigate the ability of ligand (T3) to dissociate NCoR and recruit TRAP220. *p<0.05, **p< 0.01, ***p<0.001, ***p<0.0001 for comparisons of WT vs TRα mutants. **(b)** Analysis of KLF9 expression in patient-derived primary cells containing WT TRα or the E403X and E403K mutant TRα receptors. *p< 0.05, **p<0.01 for comparisons of E403X vs E403K mutant TRα. **(c)** Electrophoretic mobility shift assays with WT, E403X or E403K mutant TRα and RXR, with a canonical thyroid hormone response element (TRE) (DR+4) or a known TRE in the human *KLF9* promoter, in the presence of 1μM T3 or 1μM ES08.

Figure 4. Comparison of wild-type and P393GX LBD structures. (a) Schematic representation of the P393GX LBD with squares representing alpha-helices, arrows beta-strands and specific features of the P393GX mutant compared to wild-type highlighted in yellow. Wild-type **(b)** and P393GX **(c)** LBD structures showing significantly different regions coloured differently, in wild-type (purple) and P393GX (yellow). Comparison of the wild-type **(d)** and P393GX **(e)** ligand binding pockets showing the different orientation of His 381 and different position and interactions of Arg 384 residues. Key residues and helices are labelled with dashed lines denoting polar contacts.

Figure 5. Characterisation of P393GX LBD. (a) Corepressor binding assay of P393GX by fluorescence anisotropy showing saturating-binding curves and dissociation constant (Kd) of the P393GX binding to corepressor peptide in the absence (blue) and presence (red) of T3. Error bars indicate ± s.e.m. (n=5). **(b)** Thermal stability (melting temperature) of P393GX in the apo form (blue), with T3 (red), with SMRT peptide (light green), and both T3 and SMRT peptide (dark green). **(c)** Purification of P393GX by GST and ion exchange chromatography illustrated in a SDS-PAGE. **(d)** 2F0-Fc Electron density map contoured at 1.0 σ around the binding pocket of the protein, clearly showing T3 and the residues conforming the ligand binding pocket.

Figure 6. Effect of T3 and analogues on binding of wild-type and mutant TRα LBDs to corepressor. **(a)** Chemical structures of T3 analogues. Three series of novel T3 derivatives are shown. Each series contains an extension at the 4' hydroxyl group of T3 linked with either an ether, ester or sulfonate ester functional group. The extensions differ in size, hydrophobicity and conformational flexibility. The JM ligands also have a carboxylic acid at the distal end of the extension. **(b)** Corepressor binding affinity (dissociation constants) in fluorescence anisotropy assays (upper graphs) and thermal stability (melting temperature) (bottom graphs) of wild-type and mutant TRα LBDs in the presence of T3 and different analogues. Anisotropy values were measured at every concentration of the protein:T3 analogue (molar ration 1:2) mixture to generate saturation-binding curves from which the equilibrium dissociation constant of the interaction (Kd) was calculated. Error bars indicate ± s.e.m. (n=3); *p< 0.05 for comparisons of TRα mutants and T3 vs TH analogues. Melting temperatures of apo receptor proteins (blue), and with T3 (red) or with T3 analogues (different colours), obtained by measuring changes in ellipticity of samples at 222 nm over a temperature range (20 to 90°C, 1 degree steps), are also shown. Error bars indicate ± s.e.m. (n=3); *p< 0.05, **p<0.01 for comparisons of TRα mutants and T3 vs TH analogues.

Figure 7. Binding affinity and fitting of ES08. (a) Competitive binding assay with radiolabelled T3, wild-type or mutant TRα and increasing concentrations of unlabelled ES08, indicating dissociation constants (Kd) obtained. Data shown are the mean ± s.e.m. from two independent experiments performed in triplicate. Note that the data for WT binding T3 is included for comparison and is duplicated from figure 2c. **(b)** Model of corepressor binding to P393GX:T3 complex. T3 is shown in green with the SMRT corepressor peptide in red. Interaction of the LDB and corepressor peptides is mediated by corepressor recruitment in a hydrophobic groove formed by H3 and H5 of the LDB. Due to the lack of H12 in mutants TRα, there is no disruption of the CoR binding surface and the corepressor remains interacting with the mutant receptors even in the presence of T3 forming the ternary complex. **(c)** Model of ES08 (cyan) binding to P393GX. In contrast to T3, the extension at the

4'-hydroxyl of the outer thyronine ring potentially disrupts the CoR binding surface of the LBD and, consequently, interferes with corepressor interaction.

Figure 8. Interaction of VP16-TRα with GAL4-Corepressor in mammalian cells. (a) Schematic representation of the cellular two-hybrid assay (left) and different human GAL4-Corepressor isoforms (with locations of nuclear receptor interaction domains, red) tested (right). Below this interaction of WT or mutant VP16-TRα fusions with different corepressor isoforms in absence (blue) or presence (red) of T3 is shown. Results are mean ± s.e.m. of at least 5 independent experiments performed in triplicate; *p< 0.05, **p< 0.01, ***p<0.001 for 0nM T3 vs 10nM T3 comparisons. **(b)** Interaction of GAL4-NCOR-δ with VP16-WT or mutant TRα fusions in the presence of vehicle (DMSO), 100nM T3 or different analogue. Results from at least 5 independent experiments are shown as a percentage of interaction of WT or TRα mutants with NCoR-δ with vehicle; *p< 0.05, **p< 0.01, ***p<0.001 for comparisons of TRα mutants and T3 vs TRα mutants and analogue; #p<0.001 for comparison of WT vs TRα mutants with 100nM T3.

Figure 9. ES08 induces greater dissociation of corepressors from E403X mutant TRα than T3 but fails to recruit Gal4-TRAP220 coactivator in cellular protein interaction assays. (a) Dissociation of VP16-WT or VP16-E403X mutant TRα from GAL4-NCOR-δ with increasing concentrations (0-10,000nM) of T3 or ES08. Results shown as Relative Luciferase Units (RLU) normalized to β-galactosidase activity are the mean ± s.e.m. of at least 5 independent experiments performed in triplicate. *p< 0.05, **p< 0.01, ***p< 0.001, ****p< 0.0001 for comparison of E403X plus T3 vs E403X plus ES08. **(b)** Interaction of VP16-E403X mutant TRα with different Gal4-corepressor isoform fusions in the absence of ligand (white bar), 1000nM T3 (black bar) or ES08 (red bar). Results from at least 5 independent experiments performed in triplicate are expressed as a percentage of WT TRα-corepressor interaction in absence of T3. *p< 0.05, **p< 0.01 for comparison of E403X plus T3 vs E403X plus ES08. **c)** Inability of VP16-E403X mutant TRα (red line) to recruit GAL4-TRAP220

coactivator fusion over a range (0-10,000nM) of T3 or ES08 concentrations. The data are expressed as fold induction, relative to cells transfected with Gal4-TRAP220 and VP16 alone and are the mean ± s.e.m. of at least 5 independent experiments each undertaken in triplicate.

Figure 10. Effect of T3 and ES08 on E403X mutant TRα expressing zebrafish embryos and E403X TRα mutation-containing, patient-derived inducible pluripotent stem cells. Panels (a) and (b): normal or abnormal morphology of embryos injected with hTRα WT or hTRα E403X mRNAs, at 3 days post fertilization (dpf). Cerebral oedema (ce), pericardial oedema (pe) altered body curvature (bc), and thickening of caudal vein plexus (cvp), were used to calculate an abnormal morphology index (AMI, 0= unaffected, 1-4=affected). Scale bar = 250 μm. Boxplots of AMI of WT (open) or E403X injected zygotes treated with DMSO (grey), T3 (purple) or ES08 (grey-green) are shown in **Panel (c)**. **Panels (d) and (e):** the transgenic line *tg*(*kdrl*:EGFP) was used to visualize normal or disrupted vascular architecture of the trunk-tail region of embryos at 4 dpf (in lateral view, head to the left). Anomalies including incomplete vessel (iv), aberrant branching (ab), misplaced vessel (mv), and reduced caudal vein plexus (cvp) area shown in Panel (e) were used to calculate a vascular malformation index (VMI 0=unaffected, 1-4=affected). Scale bar = 50 μm. Boxplots of VMI of WT and E403X injected zygotes treated with DMSO (grey), T3 (purple) or ES08 (grey-green) are shown in **Panel (f)**. **Panels (g-j):** normal or defective cranial cartilage development and bone mineralization in 5dpf embryos stained with Alcian Blue (in blue) and Alizarine (in red), respectively. Absent or reduced mineralization of cleitrum (cl) and operculum (op) (visible in lateral view), and malformations of ceratohyal (ch) and the five ceratobranchial (cb) arches cartilages (visible in ventral view) were quantified to compute a skeletal malformation index (SMI). Scale bar = 100 μm. **Panel (k):** Box plots of SMI of WT and E403X mutant TRα expressing embryos following exposure to DMSO (grey), T3 (purple) or ES08 (grey-green). Indices shown are mean+/-sem of pools of 60 embryos per condition, from at least 4 independent experiments. $p<0.001$ (***) for comparison of malformation indices in E403X TRα expressing embryos after exposure to DMSO versus ES08.

Figure 11. In vivo analysis of TRα target genes. Panels (a) and **(b)**: Expression of thyroid hormone receptor target genes (KLF9 and Dio3b) in WT and E403X mutant TRα-injected zygotes exposed to vehicle (DMSO), T3 or ES08. Results are expressed as fold changes vs DMSO-treated cells. *p< 0.05, **p< 0.01 for comparison with vehicle-treated embryos. **Panel (c):** Expression KLF9 (a thyroid hormone receptor target gene) in inducible pluripotent stem cells derived from patient harbouring E403X TRα mutation, with increasing concentrations of T3 (blue bar) or ES08 analogue (red bar). Results are expressed as fold changes vs non-treated cells: *p< 0.05, **p< 0.01 for comparison of E403X with T3 vs E403X with ES08.

Table 1. Data collection and refinement statistics.

The table indicates the data collection and refinement statistics generated for the P393GX:T3 model. The number of crystals for this structure is one. R.M.S., root mean square. Values in parentheses are for the highest-resolution shell.

Figure 1

A

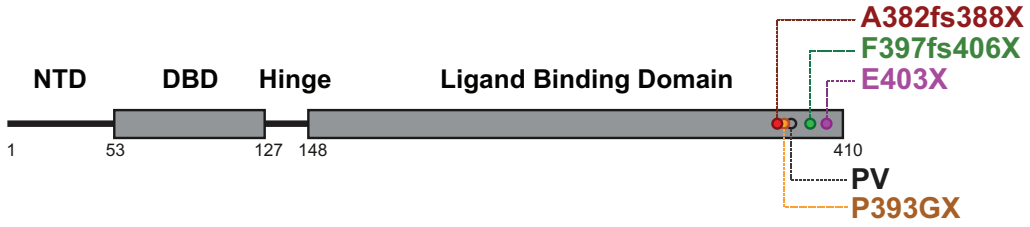

B

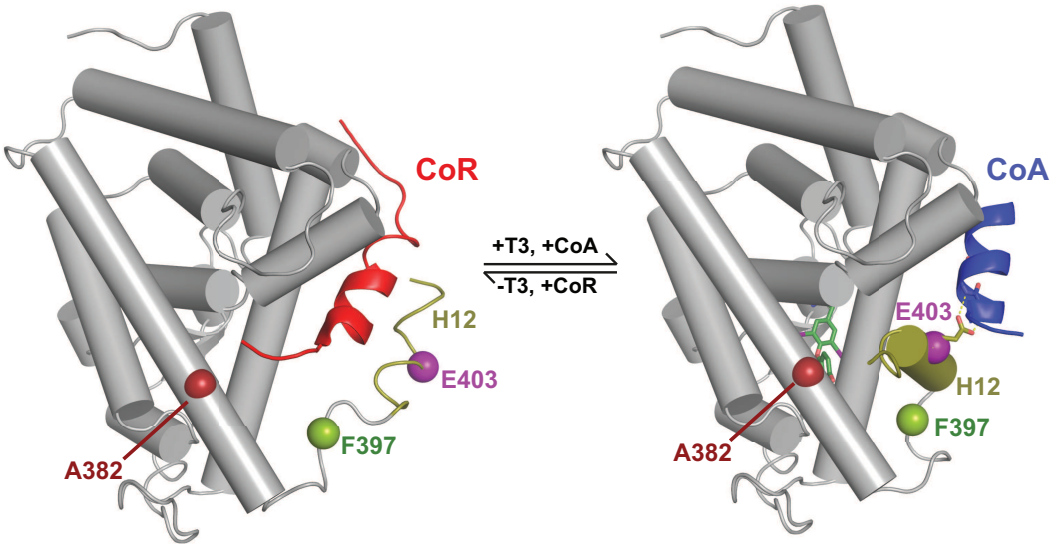

Figure 2

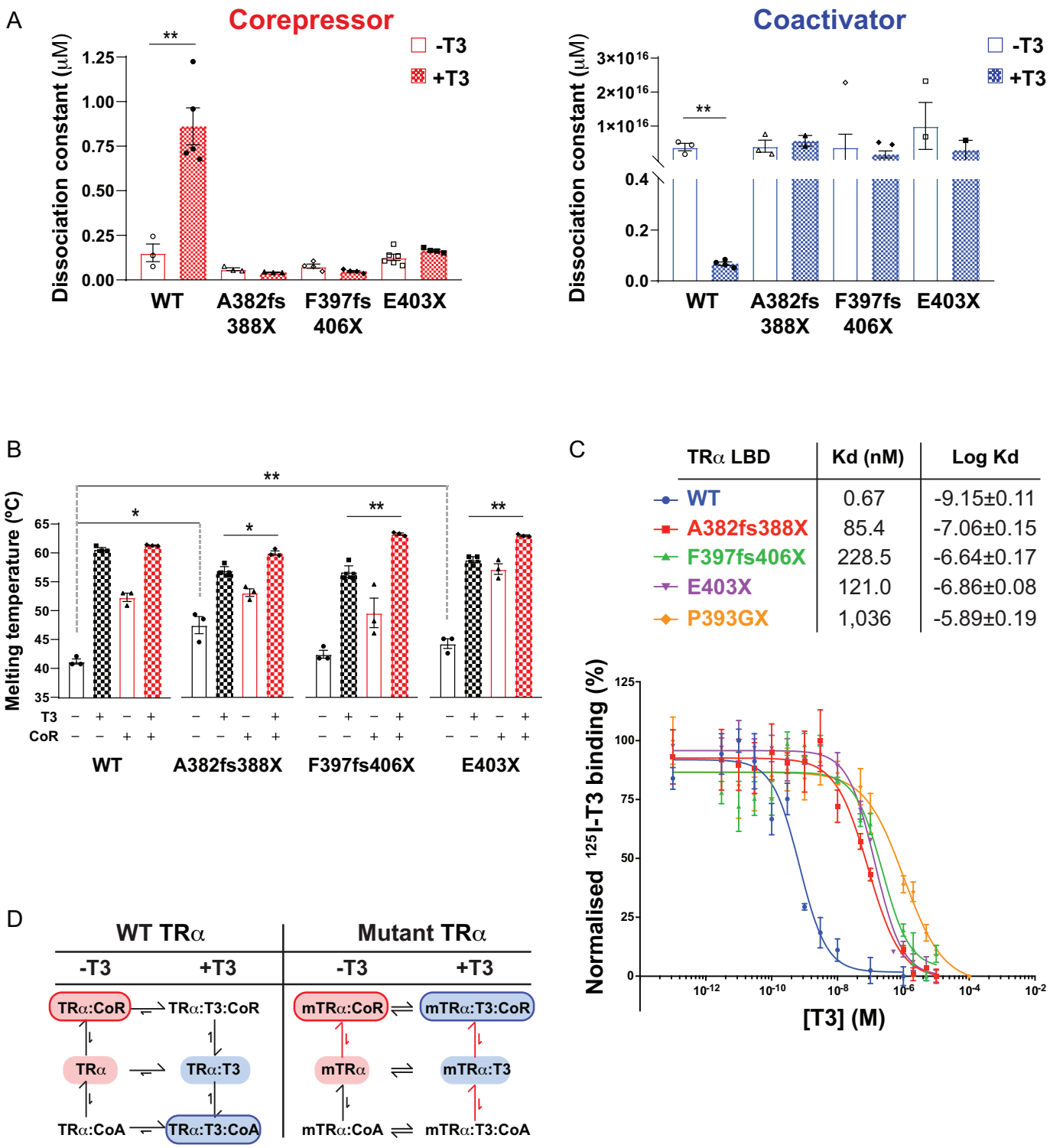

Figure 3

A

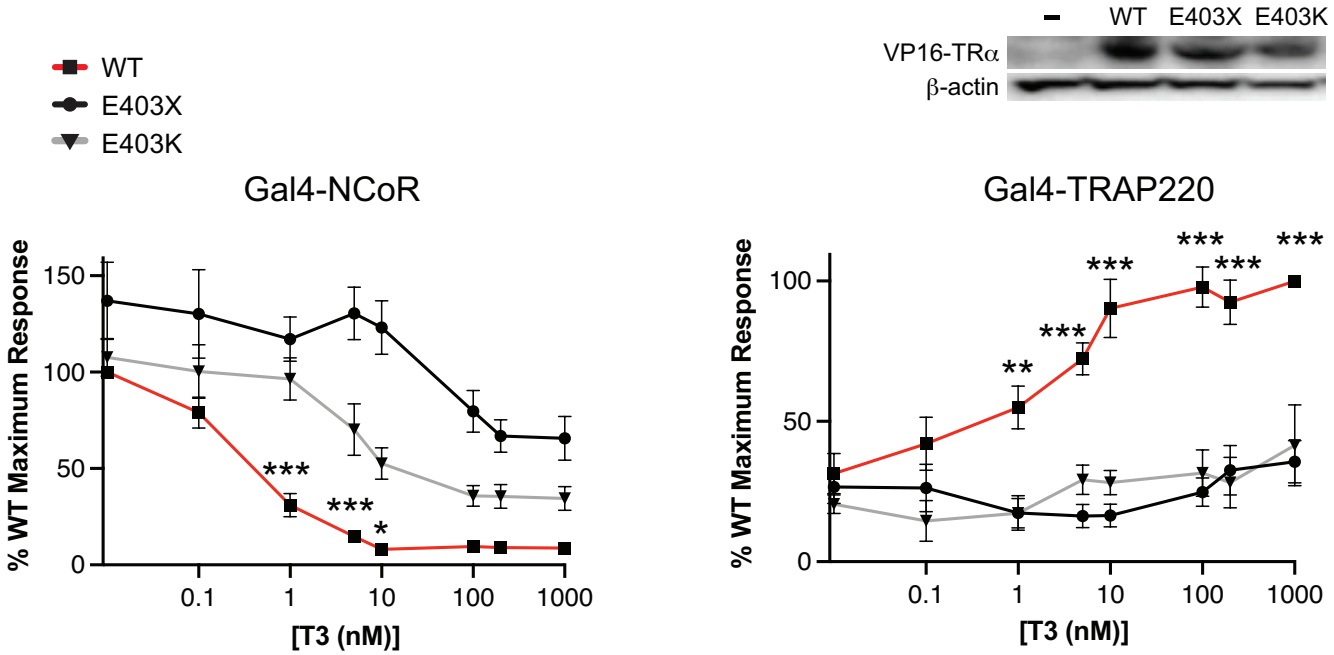

B

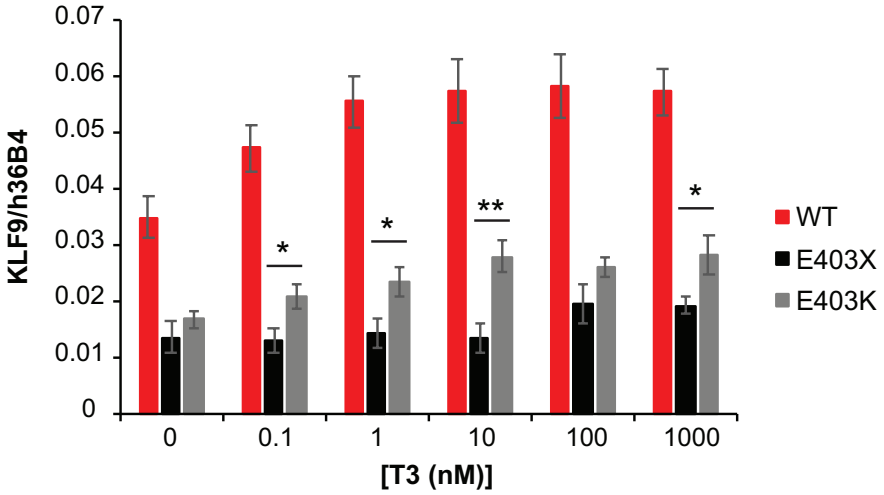

C

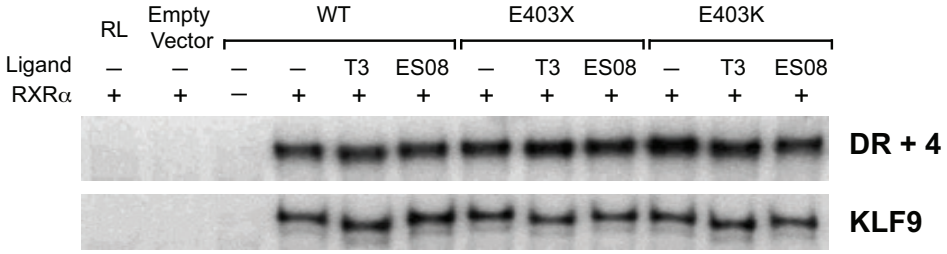

Figure 4

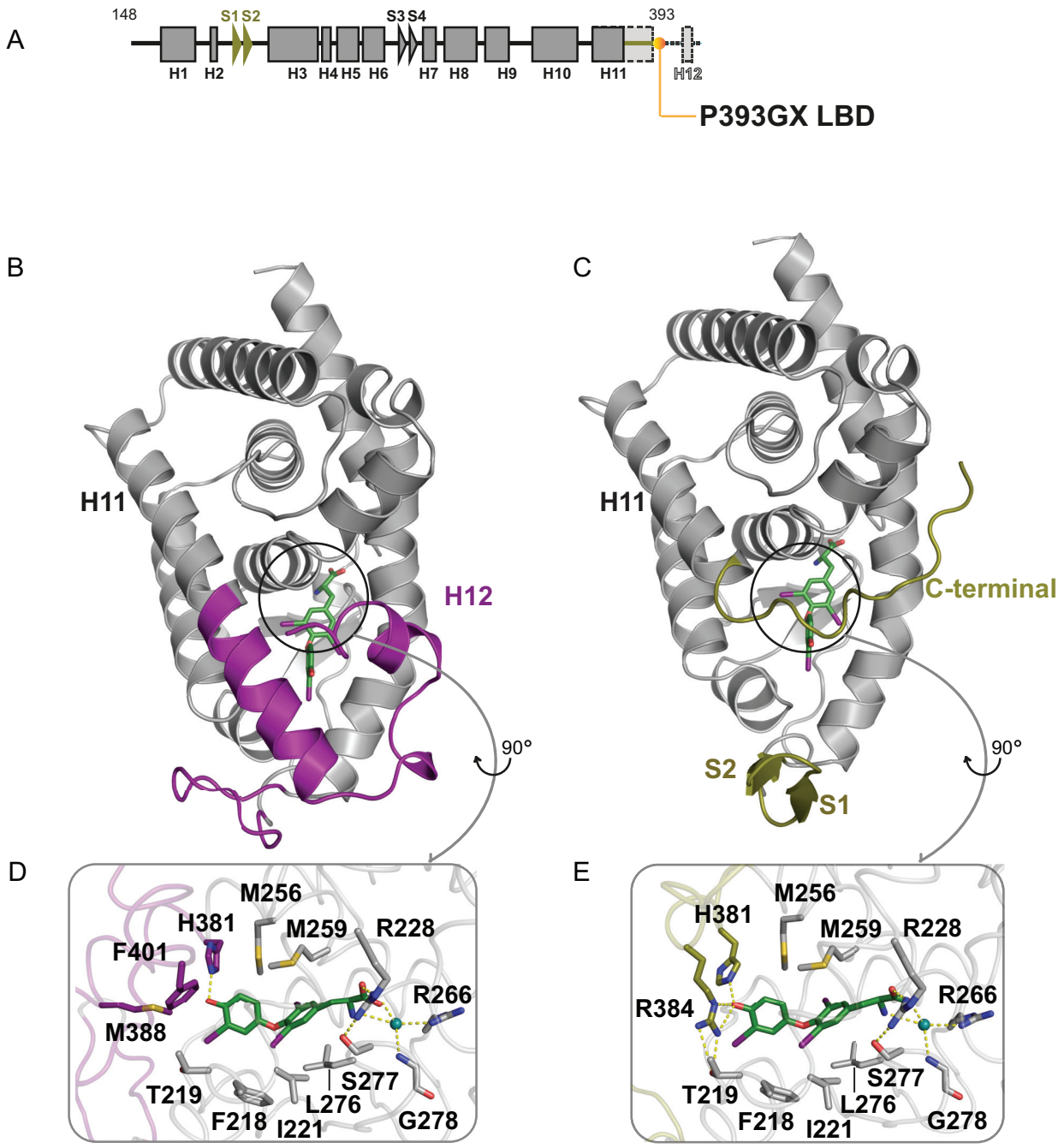

Figure 5

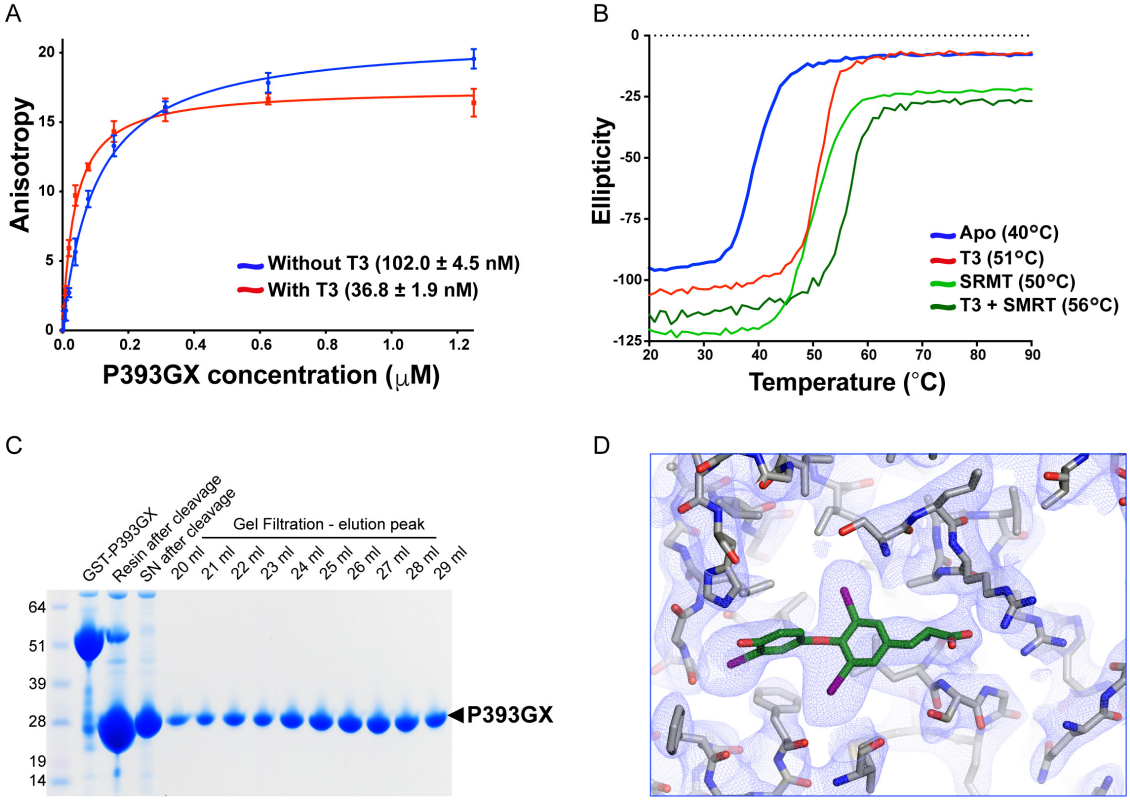

Figure 6

A

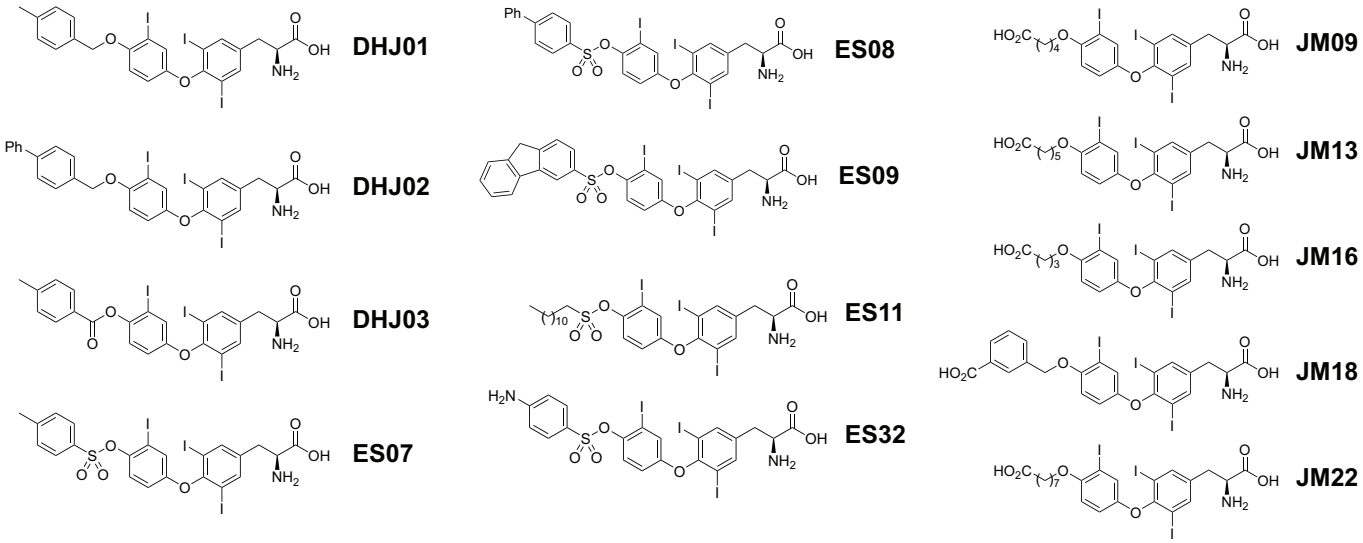

B

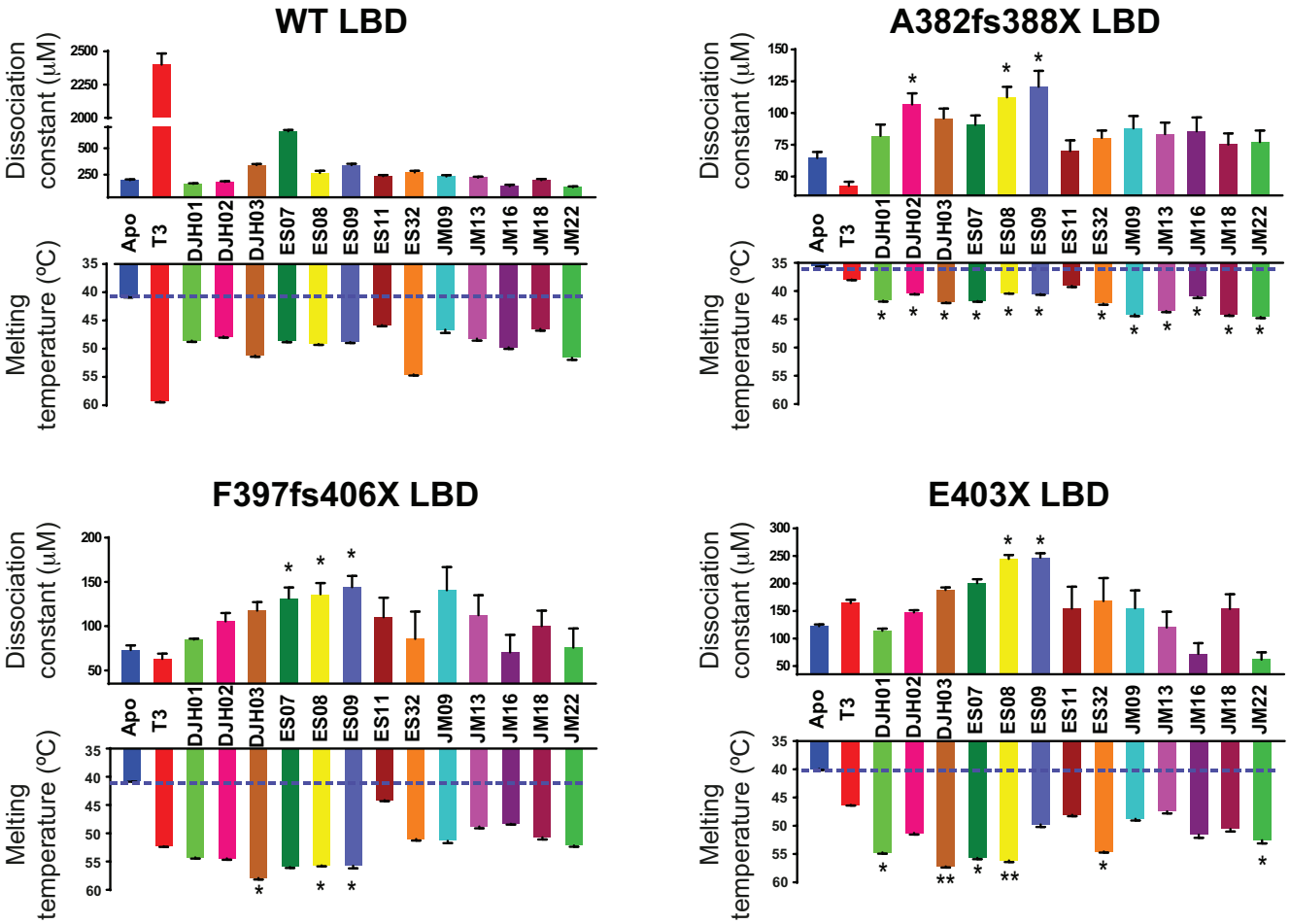

Figure 7

A

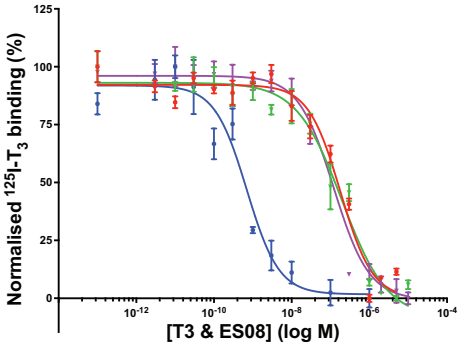

TRα LBD	Kd (nM)	Log Kd
WT & T3	0.67	-9.15±0.11
WT & ES08	180.0	-6.74±0.09
E403X & T3	121.0	-6.86±0.08
E403X & ES08	198.0	-6.70±0.13

B

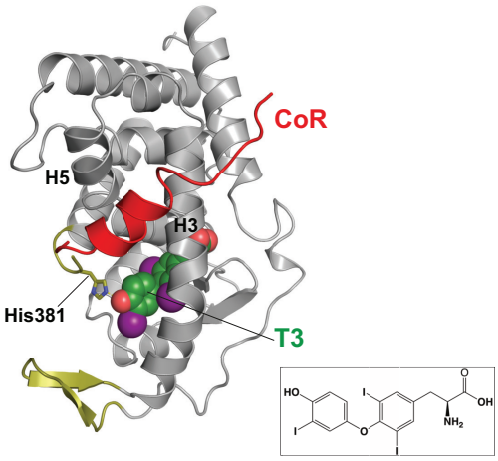

C

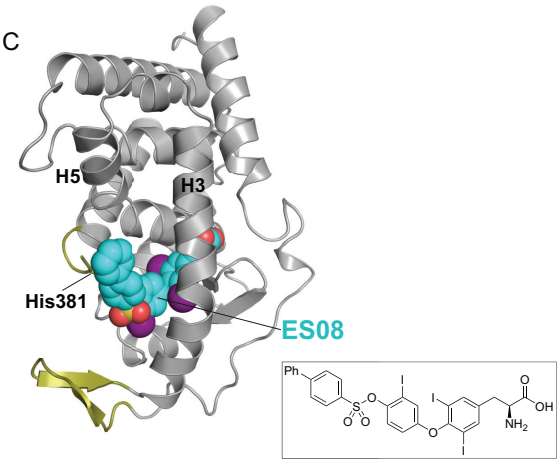

Figure 8

A

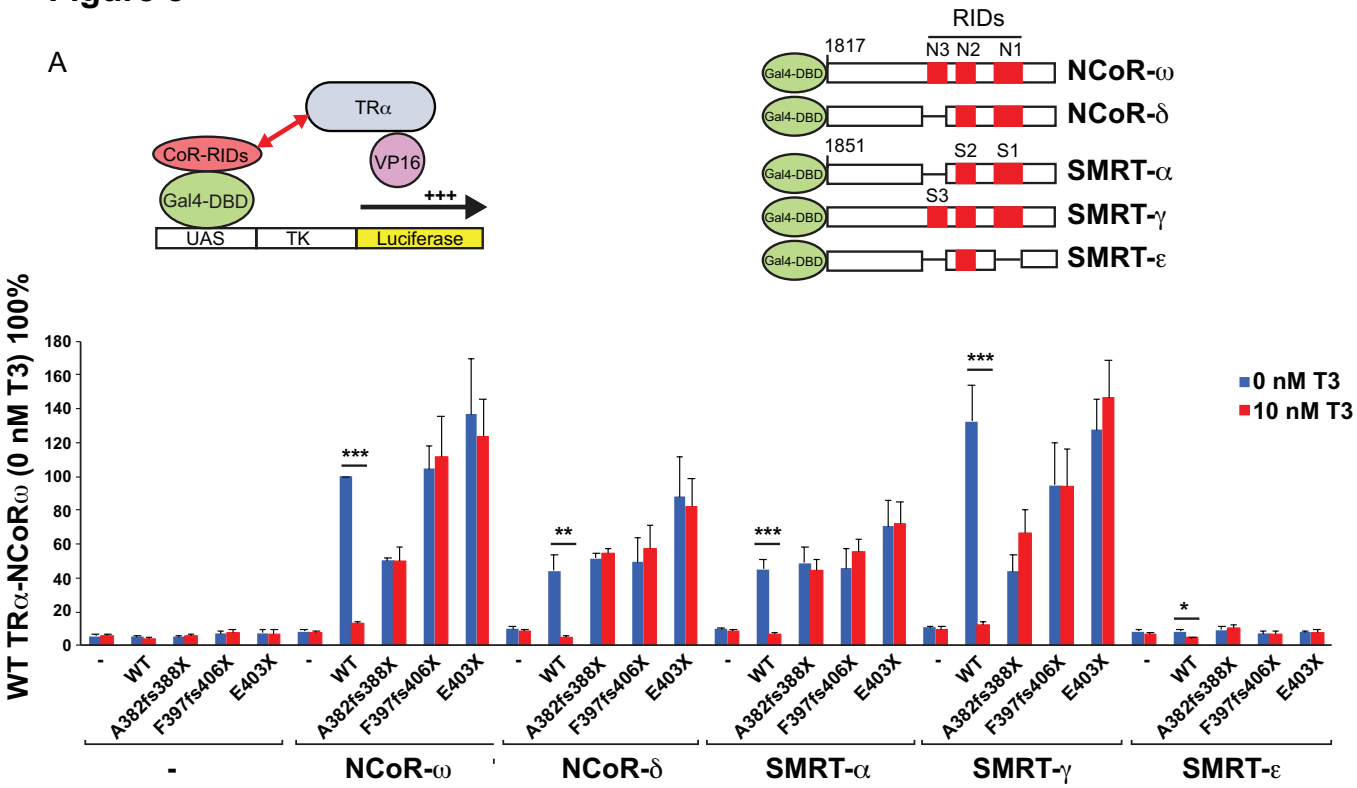

B

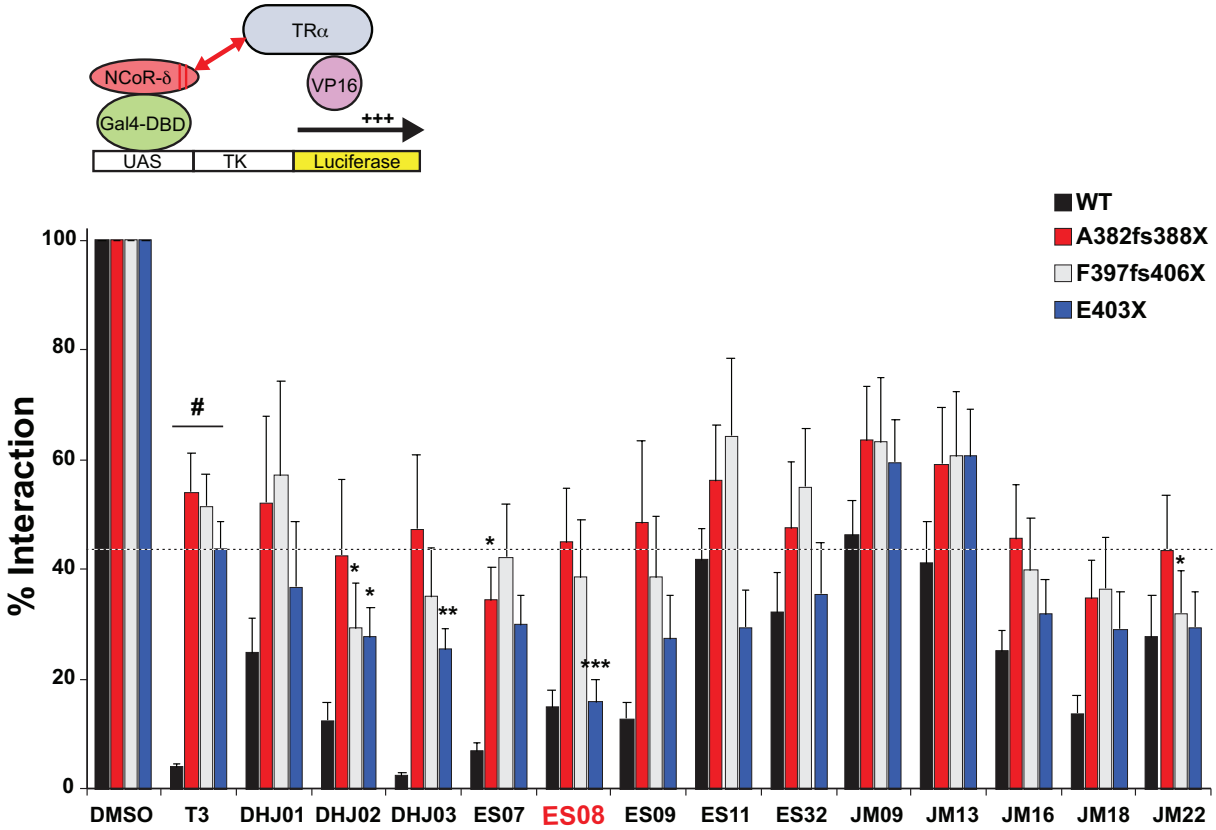

Figure 9

A

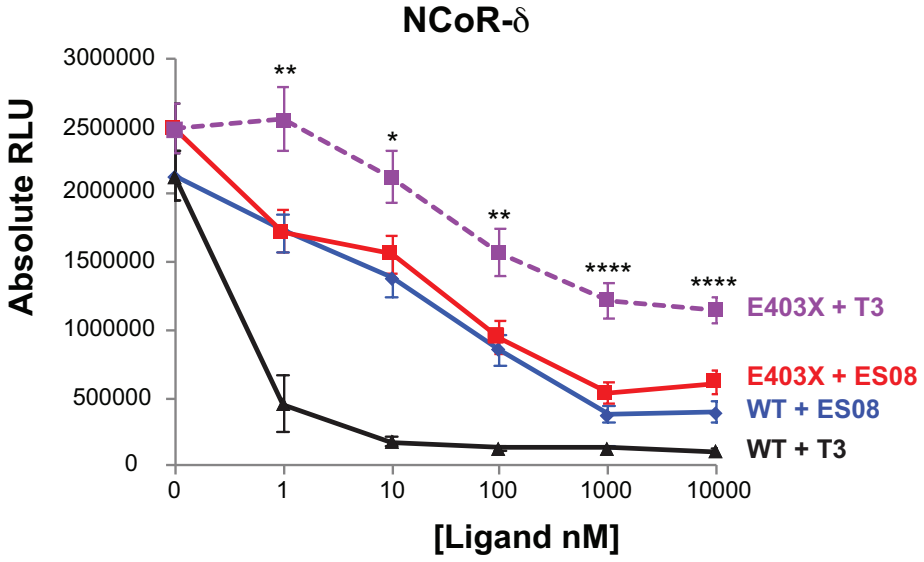

B

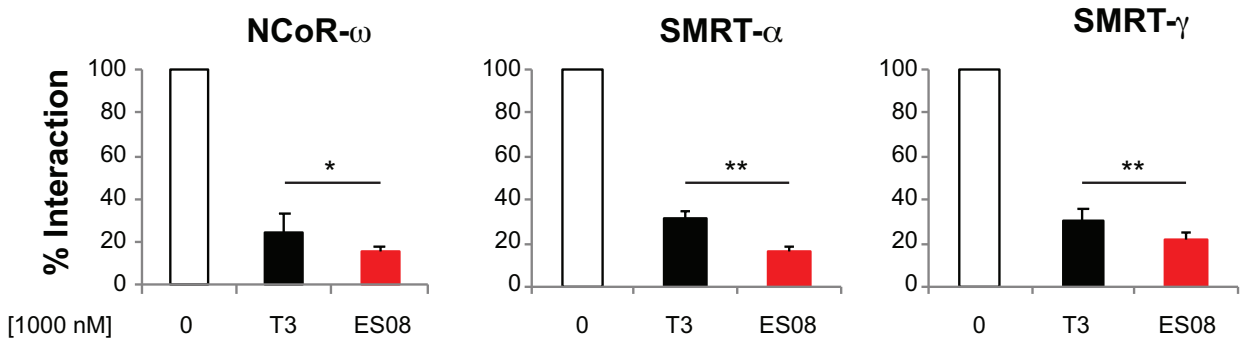

C

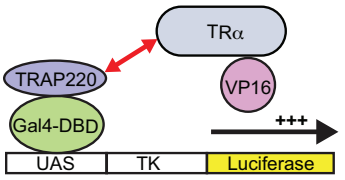

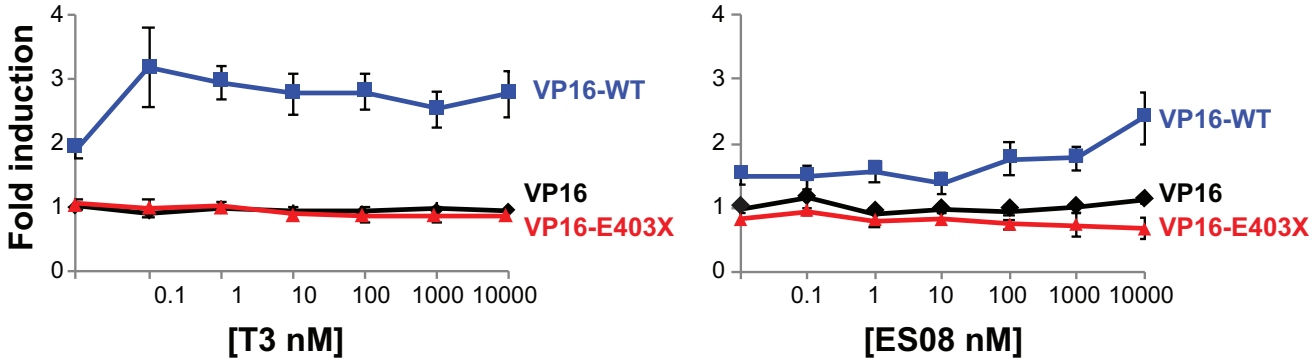

Figure 10

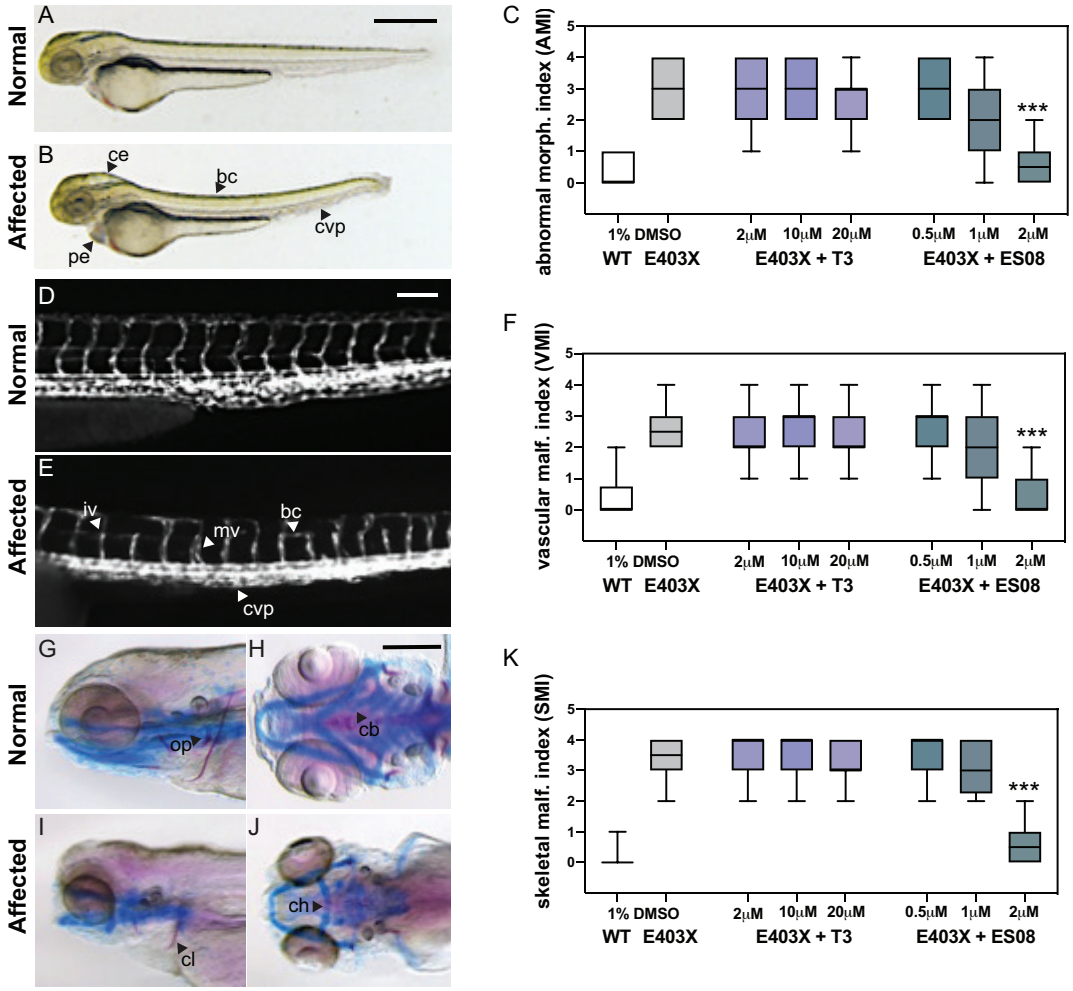

Figure 11

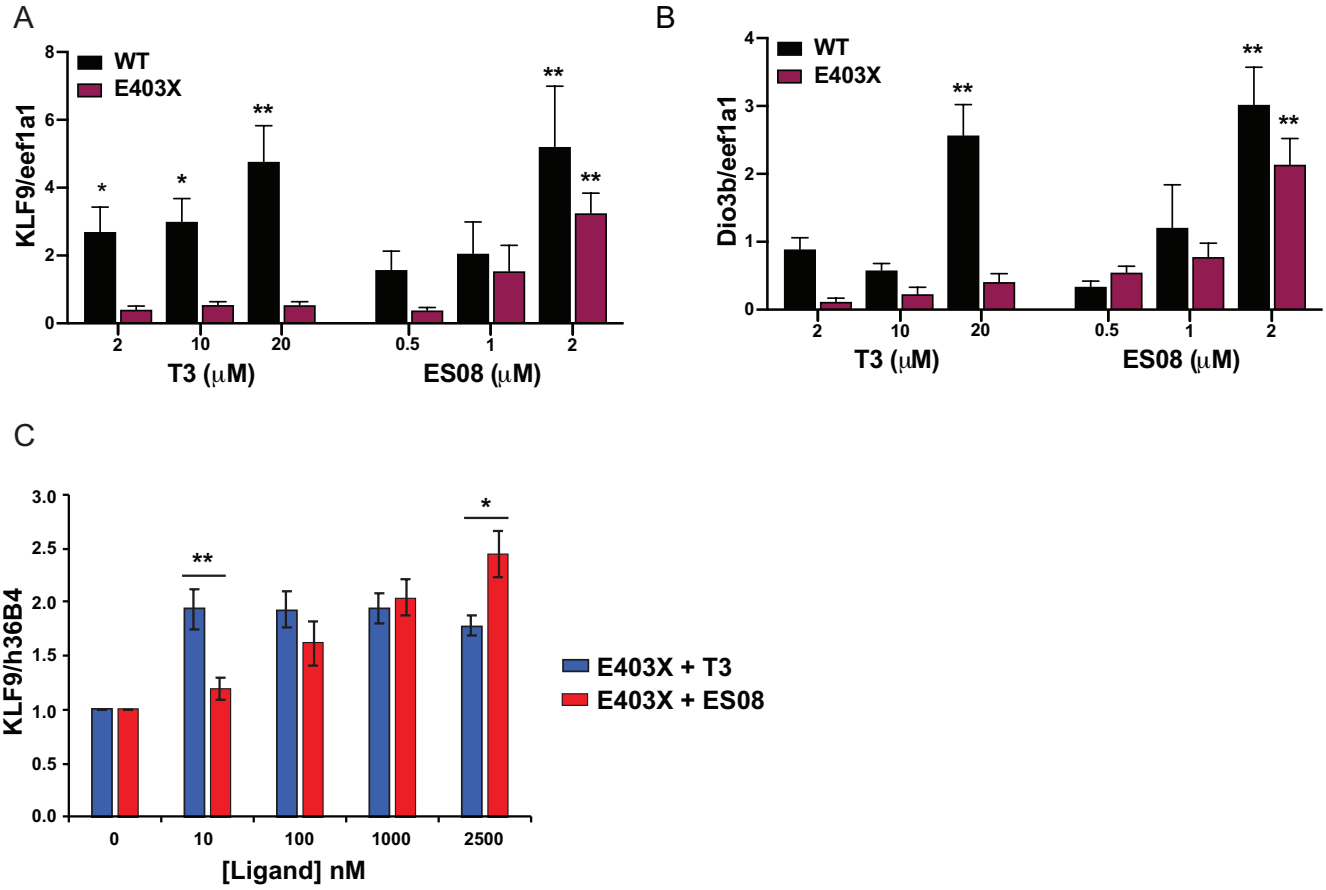

Table 1

Data collection	**P393GX: T3**
Space group	$P6_422$
Cell dimensions	
a,b,c (Å)	143.33 143.33 88.50
α, β, γ (°)	90.00 90.00 120.00
Wavelength	0.9692
Resolution (Å)	71.06 - 3.00 (3.18 - 3.00)
R_{merge}	0.130 (0.690)
$I/\sigma I$	22.0 (5.3)
Completeness (%)	100.0 (100.0)
Redundancy	16.5 (17.3)
Refinement	
Resolution (Å)	71.06 - 3.00 (3.18 - 3.00)
Total no. reflections	185125 (30547)
R_{work}/ R_{free}	0.18/0.22
No. atoms	
Protein	3824
Ligand	23
Water	9
B-factors	
Protein	60.78
Ligand	51.45
Water	40.95
RMS deviations	
Bond lengths (Å)	0.0164
Bond angles (°)	2.0587